Factors influencing magmatism during continental breakup: New insights from a wide-angle seismic experiment across the conjugate Seychelles-Indian margins

J. S. Collier,[1] T. A. Minshull,[2] J. O. S. Hammond,[3] R. B. Whitmarsh,[2] J.-M. Kendall,[3] V. Sansom,[1] C. I. Lane,[2] and G. Rumpker[4]

Received 26 June 2008; revised 3 November 2008; accepted 4 December 2008; published 4 March 2009.

[1] We present a model of the northern Seychelles continental margin derived from controlled source, wide-angle seismic traveltime inversion and teleseismic receiver functions. This margin has been widely cited as a classic example of rifting in association with a continental flood basalt province, the Deccan Traps. However, we do not find the typical set of geophysical characteristics reported at other margins linked to continental flood basalts, such as those of the north Atlantic. The oceanic crust formed immediately after breakup and throughout the first 3 Ma of seafloor spreading is just 5.2 km thick, less than half that typically seen at other volcanic margins. The continent-ocean transition zone is narrow and while two packages of seaward-dipping reflectors are imaged within this transition they are weakly developed. Beneath the thinned continental crust there is an approximately 4 km thick layer of high-velocity material (7.5–7.8 km/s) that we interpret as mafic material intruded and underplating the lower crust. However, we believe that this underplating most likely happened prior to the breakup. Overall the observations show that the rifting of India from the Seychelles was characterized by modest magmatism. The spatial extent of the Deccan flood basalt province is therefore smaller than previously thought. We speculate that either the lateral flow of Deccan-related hot material beneath the breakup region was hampered, perhaps as the rifted margins did not intersect the center of the Deccan source, or there was incomplete melt extraction from the wide melting region that formed between the rapidly diverging plates. If the latter explanation is correct, then the rate of plate separation, as indicated by the initial seafloor-spreading rate, is more important in controlling the volume of magmatism generated during continental rifting than has been previously recognized.

Citation: Collier, J. S., T. A. Minshull, J. O. S. Hammond, R. B. Whitmarsh, J.-M. Kendall, V. Sansom, C. I. Lane, and G. Rumpker (2009), Factors influencing magmatism during continental breakup: New insights from a wide-angle seismic experiment across the conjugate Seychelles-Indian margins, *J. Geophys. Res.*, *114*, B03101, doi:10.1029/2008JB005898.

1. Introduction

[2] In the 1980s and 1990s, studies of rifted continental margins established two end-member types depending on the degree of rift-related magmatism, the so-called volcanic and nonvolcanic margins [*Mutter et al.*, 1988; *White*, 1992a]. Volcanic margins are characterized by seaward-dipping reflectors corresponding to thick subaerial and shallow marine lava flows, high seismic velocity (>7.2 km/s) bodies in the lower crust, formed by igneous rocks that intruded and/or underplated the thinned continental crust and thick early oceanic crust (up to twice the normal ~7 km thickness for the first ~5 Ma of seafloor spreading). In contrast, nonvolcanic margins are characterized by 5–20 km wide, tilted, continental blocks bounded by large seaward-dipping normal faults, areas of exhumed subcontinental mantle [*Whitmarsh et al.*, 2001] and/or thin early oceanic crust. Many volcanic margins were shown to be spatially and temporally linked to onshore flood basalt provinces and offshore, to aseismic ridges linking them to present-day hot spots. On the basis of this association, it was suggested that the excess magmatism could be entirely explained by decompression melting of passively upwelling hot asthenosphere, or mantle plume head, beneath the thinning lithosphere [*White and McKenzie*, 1989]. In the north Atlantic, the region where many of the current ideas about continental breakup developed, the application of this passive melting model to explain the observed melt volumes implies that the Iceland plume increased mantle temperatures by 150°C

[1]Department of Earth Science and Engineering, Imperial College London, London, UK.
[2]National Oceanography Centre, University of Southampton, Southampton, UK.
[3]Department of Earth Sciences, University of Bristol, Bristol, UK.
[4]Arbeitsbereich Geophysik, Johann Wolfgang Goethe Universitat, Frankfurt, Germany.

0148-0227/09/2008JB005898$09.00

along a 2000 km length of rift [*Barton and White*, 1997]. Following breakup, elevated temperatures were maintained only in the ~200 km wide immediate plume region to form the Greenland-Iceland-Faeroe Ridge, and elsewhere the thermal anomaly decayed and the oceanic crust thickness reached normal values after 5–10 Ma. It has been suggested that this decay might be explained by the presence at breakup time of an exhaustible hot layer at the top of the asthenosphere [*Nielsen and Hopper*, 2004; *Armitage et al.*, 2008].

[3] However, not all volcanic margins have conclusive evidence for the presence of a mantle plume at the time of rifting, most notably the Australian Cuvier margin [*Hopper et al.*, 1992] and Eastern United States margins [*Holbrook et al.*, 1994a, 1994b]. These examples led to a second group of models in which the excess volcanism was explained by small-scale convection in the upper mantle generated at the time of rifting, without the need for a mantle thermal anomaly at all. Active upwelling increases the throughput of asthenosphere and hence the volume of melt generated by decompression partial melting [*Mutter et al.*, 1988; *van Wijk et al.*, 2001]. The proponents of this model argued that it better explained the transient nature of the magmatic anomaly and suggested that the generation of local convection is encouraged by rapid rifting and a narrow rift zone, both thought to be characteristics of volcanic as opposed to nonvolcanic margins. Unfortunately, while there have been many attempts to generate small-scale convection by numerical simulations, a consensus as to the conditions required to initiate it has not been reached [*Sleep*, 2007]. More recently, other workers have proposed a third scenario, in which decompression melting of passively upwelling warm asthenosphere and active convection act *together* to produce the observed excess magmatism [*Kelemen and Holbrook*, 1995; *Keen and Boutilier*, 2000]. Applying this idea to the case of the north Atlantic margins, *Holbrook et al.* [2001] estimated the mantle temperature was just 100°C hotter than normal beneath the entire province, but with significant active upwelling within 300 km of the Iceland plume compared to only passive upwelling in the more distal regions.

[4] In this paper we present results from a seismic experiment conducted across the north Seychelles continental margin carried out as part of a larger study of the conjugate north Seychelles-Laxmi Ridge margins (Figure 1a). The western Indian continental margin, was one of the first to reveal seaward-dipping reflectors [*Hinz*, 1981], and the rifting of the Seychelles from the Indian subcontinent has been widely linked to the eruption of the Deccan Trap flood basalt province at 65.5 ± 1 Ma [*Courtillot and Renne*, 2003]. The origin of the Deccan has been attributed to both a mantle plume (that later built the Chagos-Laccadive and Mascarene ridges and today resides below Réunion [*Richards et al.*, 1989; *White and McKenzie*, 1989; *Duncan et al.*, 1990]) and edge-driven convection induced by lateral variations in lithospheric thickness beneath the Indian subcontinent and surrounding ocean basins [*Anderson*, 1994]. The timing of flood basalt emplacement and breakup are well constrained [*Collier et al.*, 2008] and, irrespective of the origin of the Deccan traps, our study area is a clear, undisputed example of associated continental flood basalt province and continental rifting. The Seychelles-Indian margins therefore provide an ideal opportunity to test our current understanding of the factors which influence the volumes of magma generated during continental breakup that have been largely developed from observations in the Atlantic.

2. Study Area

[5] Spectacular exposures of granite led *Wegener* [1924] to first propose that the Seychelles Islands and Plateau were of continental origin. This was confirmed in the late 1950s/early 1960s when seismic refraction profiles collected with sonobuoys found a thick crust with a continental-like velocity profile that was surrounded by oceanic crust on three sides [*Gaskell et al.*, 1958; *Shor and Pollard*, 1963; *Davies and Francis*, 1964; *Francis et al.*, 1966; *Francis and Shor*, 1966] (Figure 1b). No crustal-scale controlled source seismology has been conducted in the region since this time, and the crustal affinity of the part of the Mascarene Plateau that lies to the southeast of the Seychelles Plateau remains unknown. The Mesozoic sediments on the Seychelles Plateau itself however were more recently the focus of hydrocarbon exploration activity that resulted in the collection of an extensive seismic reflection and magnetic data set and the drilling of four deep wells [*Plummer*, 1994].

Figure 1. (a) Satellite gravity of the northwest Indian Ocean [*Sandwell and Smith*, 1997] showing location of conjugate Seychelles-Laxmi Ridge margin survey lines. (b) Bathymetry of the Seychelles Plateau and surrounding areas (1 km contour interval, ETOPO5, National Geophysical Data Center, 1993). SP, Seychelles Plateau; MP, Mascarene Plateau. The bold black line marks the Seychelles wide-angle model line presented here and the box marks the area shown in Figure 2. Numbered dark gray circles and dark gray lines are historical sonobuoy wide-angle seismic surveys that determined continental crust beneath the Seychelles Plateau and oceanic crust elsewhere [*Davies and Francis*, 1964; *Francis et al.*, 1966; *Shor and Pollard*, 1963; *Francis and Shor*, 1966]. Numbered light gray triangles are Deep Sea Drilling Program/Ocean Drilling Program holes, and unnumbered light gray triangles are commercial holes. (c) Plate reconstruction using the 27ny Euler rotation pole of *Royer et al.* [2002] (latitude 18.83°, longitude 24.86° angle 35.411°). The Seychelles-Mascarene block is defined by the 1 and 3 km bathymetric contours, and the Indian block is defined by the 200 m bathymetric contour and coastline and the Laxmi Ridge (LR) block by gravity data [*Miles and Roest*, 1993]. GR, Gop Rift; CR, Indian Continental Rise [*Malod et al.*, 1997]. In the reconstruction the Seychelles-Mascarene block is held fixed and the Indian and Laxmi Ridge continental blocks (maintained in their present-day relative positions) are rotated back toward it. The Mascarene Plateau is shown dashed as most, if not all, of it may have formed after breakup (as indicated by ages of recovered volcanics from the holes marked with triangles [*Duncan and Hargraves*, 1990]). The white star marks the eruptive center of the Deccan Traps inferred by *Hooper* [1990], and the dashed circle has a 1000 km radius about this point. The bold black line marks the conjugate pair of velocity models shown in Figure 8.

[6] The geographic isolation of the Seychelles resulted from three phases of rifting: first by the opening of the Western Somali Basin in the mid-Jurassic (~160 Ma), second by the opening of the Mascarene Basin in the mid-Cretaceous (~84 Ma) and finally by the opening of the Eastern Somali Basin/Arabian Sea at the end of the Late Cretaceous (~62 Ma [*Norton and Sclater*, 1979]). At the time of this final rifting phase, current plate reconstructions of the north Indian Ocean place the Seychelles Plateau adjacent to the section of the Indian-Pakistan continental margin known as the Laxmi Ridge [*Todal and Edholm*, 1998; *Royer et al.*, 2002] (Figure 1c). The Laxmi Ridge, with its distinctive 25–50 mGal negative free-air gravity anomaly, was first identified by *Naini and Talwani* [1982] who proposed that it was also a continental fragment that rifted from mainland India by the opening of the Gop Rift prior to rifting from the Seychelles.

[7] Our preferred plate reconstruction [*Royer et al.*, 2002], which accounts for ridge propagation events at the Carlsberg ridge and hence seafloor-spreading asymmetry in the Eastern Somali Basin and Arabian Sea, aligns the northwestern tips of the Laxmi Ridge and Seychelles Plateau (Figure 1c). This alignment is consistent with the inferred presence of a major transform plate boundary between Greater India (India + Seychelles) and the African plate at this location in the Late Cretaceous [*Plummer*,

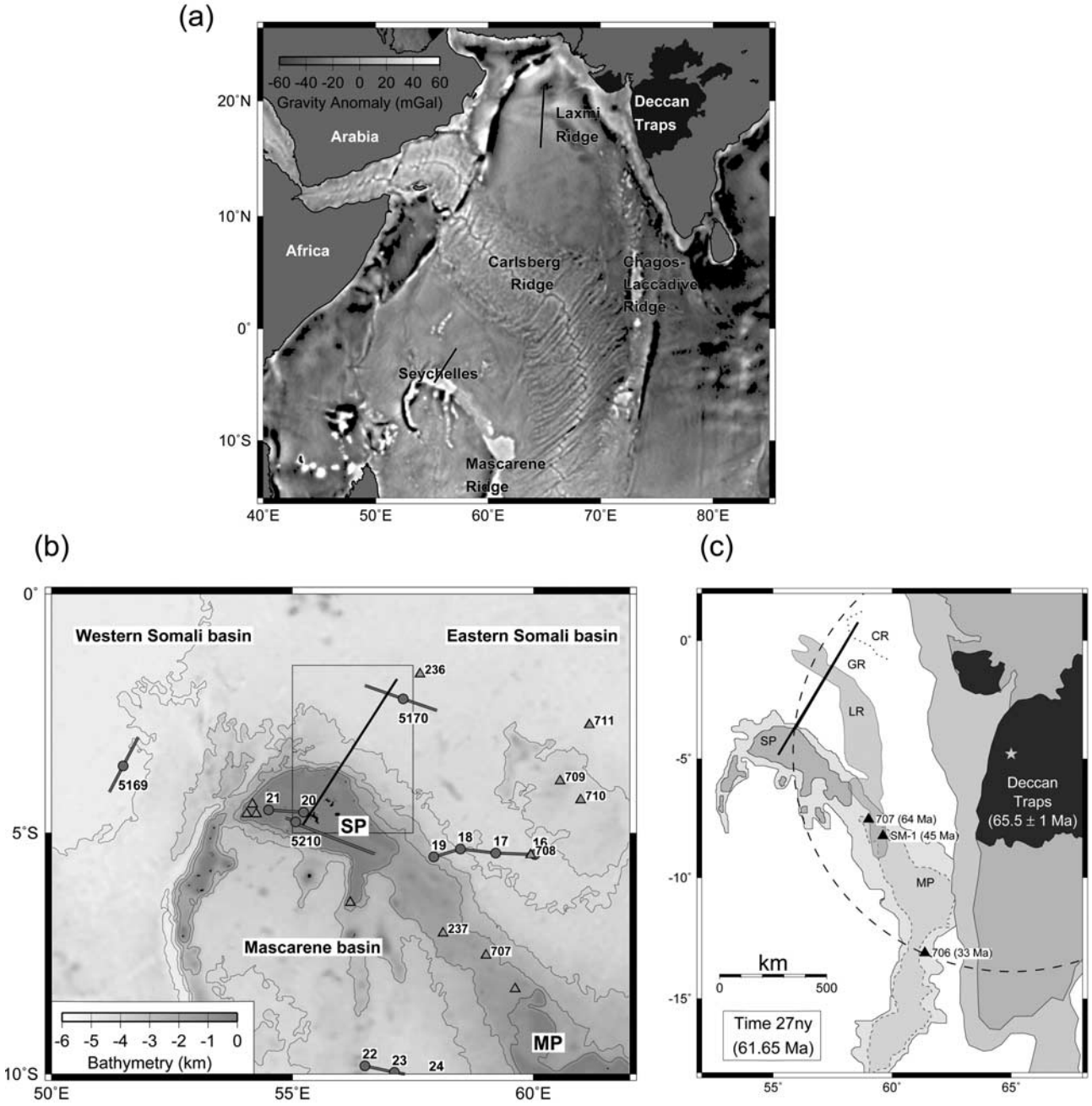

Figure 1

1996]. The reconstruction also matches three clear segments of seafloor-spreading anomaly 27n immediately north of the Seychelles and south of the Laxmi Ridge [*Collier et al.*, 2008]. We therefore believe this reconstruction to be an accurate representation of the breakup geometry, and it places our study area approximately 1000 km from the eruptive center of the Deccan, as inferred by *Hooper* [1990]. We estimate that the uncertainty in the position of the Deccan center is less than ±100 km in the direction of our study area because of the requirement to fit with the location of the offshore Laccadive Ridge to the south, which in both plume and nonplume models is considered to have formed from the Deccan source. Therefore, by analogy with the margins that border the north Atlantic, we would expect the Seychelles margin to display distal volcanic margin characteristics.

[8] Our investigation of the north Seychelles margin was conducted in three distinct phases: swath/magnetic reconnaissance in 2001 (*RRS* Charles Darwin cruise 134b), the main controlled source seismic experiment in 2003 (*RRS* Charles Darwin cruise 144) and passive seismic recording in 2003–2004 [*Hammond et al.*, 2005]. During the main, controlled source stage of our study both the Seychelles margin and the conjugate Laxmi Ridge margin were surveyed. In this paper we present the Seychelles wide-angle results. Wide-angle results from the Laxmi Ridge margin are presented by *Minshull et al.* [2008]. An analysis of the seismic reflection and magnetic data collected at the Seychelles margin in 2001 and 2003 is given by *Collier et al.* [2008].

3. Data Acquisition and Processing

3.1. Wide-Angle Data

[9] The ship tracks of our 2003 Seychelles experiment are shown in Figure 2. The main seismic transect (lines 7 and 9) was sited to avoid offsets in seafloor magnetic anomalies and a number of small deep water seamounts, and extends from seaward of magnetic anomaly 27n in the north, up the bathymetric slope and onto the shallow Seychelles Plateau in the south. Much of the plateau is uncharted, and so for navigational safety coupled with environmental reasons it was necessary to slightly deviate from the optimal line during shooting (line 7). This deviation was taken into account during subsequent data analysis, by excluding arrival picks affected by three-dimensional geometry/structure. The main transect was complemented by 650 km of additional multichannel reflection profiles (lines 10–21, Figure 2).

[10] The wide-angle transect was collected with a 6920 cubic inch, 14 element tuned air gun array designed to be rich in 5–10 Hz energy, fired at 13,790,000 Pa every 60 s (every 150 m at a nominal ship speed of 4.5 knots) and towed at 16 m depth. The shots were recorded by 32 Geomar ocean bottom instruments [*Flueh and Bialas*, 1996], consisting of 11 ocean bottom hydrophones (OBH) and 21 ocean bottom seismometers (OBS) equipped with a 4.5 or 15 Hz, three-component geophone plus hydrophone package, positioned 8 km apart. The conjugate Laxmi Ridge profile was collected first, so the Seychelles OBS/H stations are numbered 33–64. All deployed instruments were recovered, and only one failed to record any data (OBH37). The data were recorded with a 10 ms sample interval and had a correction for clock drift applied. The water column sound-speed profile was measured with a velocimeter to a depth of 4.3 km, and supplemented with shallow water temperature profiles collected by disposable XBTs. Traveltime picks of the direct wave were used to calculate the seabed instrument positions. These calculations were done in two dimensions, so any offline drift was not corrected for. However, the differences between the calculated (relocated) and logged shipboard drop positions were all less than 100 m, indicating minimal drift during instrument descent and so negligible error. The final record sections had a 1–20 Hz bandpass filter and a linear offset-dependent gain applied to boost the amplitude of the farthest offset arrivals.

[11] Because of the probability of high surf noise it was decided not to deploy any seabed instruments on the plateau. Instead here we used two Sparton Electronics AN/SSQ-57A disposable sonobuoys (stations SB09 and SB11), and temporary landstations on the Seychelles Islands of Mahé (stations 01, 04, and 07), Praslin (station 10) and Denis (station 19). The former two are granitic islands in the middle of the plateau, and the latter a coralline cay on the outer shelf. In order to ensure a common time base between the landstation and ship's GPS clocks the two were cross synchronized at the end of the cruise and found to be within 0.01 ms.

[12] Once the record sections for each land and marine station had been produced, traveltime picks of coherent phases were made manually approximately every 1.5–3 km (8–16 traces). For the OBS instruments picking was mostly done on the hydrophone components as they generally had better signal-to-noise ratio than the vertical geophones. In places the first water bottom multiple arrivals have higher amplitudes than their equivalent primaries, and were used to guide the picking. Picking of arrivals on the landstation records was similarly aided by the data recorded during the shooting of the other seismic lines parallel to the main transect. On the coincident multichannel seismic profile the Moho reflection was widely seen as a band of diffuse, high reflectivity up to 0.3 s TWT thick at about 8 s TWT (Figures 3b and 9a). Synthetic zero offset picks of both the top basement and Moho reflections into seabed instruments 33–61 were calculated from this profile and included with the other traveltime picks. On some of the instruments, helped by this zero offset guide, it was also possible to pick the wide-angle reflection from top basement where it crosscut the direct wave reverberation. Traveltime uncertainties of up to 250 ms were assigned to each pick by eye according to phase continuity and ambient noise levels, and in general increase with range. The minimum picking error was taken to be 30 ms, a quarter wavelength of the dominant 7.5 Hz signal. The average traveltime pick uncertainty (t_{unc}) for each phase is given in Table 1. During the modeling process, the traveltime picks and assigned uncertainties were checked by traveltime reciprocity to ensure internal consistency [*Zelt*, 1999]. This method identifies reversed shot and receiver pairs, and is a rapid way of highlighting data mispicks and/or inappropriate uncertainties. This proved particularly helpful for instruments sited on the relatively steep seafloor immediately north of the plateau (instruments 62–64), where the seabed is disturbed by sediment slumps and slides and some irregularities in the arrival times of short-range events were detected (Figure 3b). The assigned uncertainties were increased in these areas.

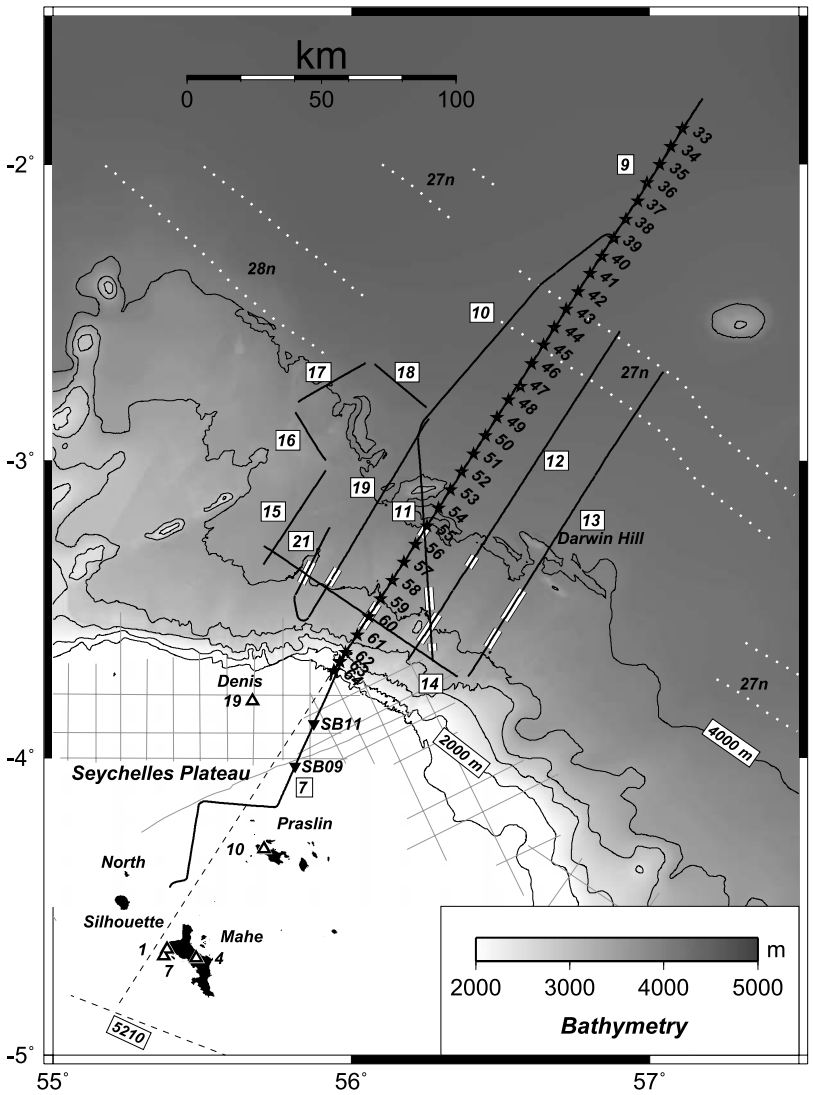

Figure 2. Bathymetric map of the study area showing locations of shooting tracks and seismic receivers. The bathymetry is a compilation of hull-mounted EM12 swath data and digitized hand-contoured unpublished historical data (R. L. Fisher, personal communication, 2003). Numbered bold black lines are seismic reflection profiles collected during CD144 (lines 7–21), and fine gray lines are commercial seismic reflection profiles on the plateau. White bars are identified seaward-dipping reflectors from *Collier et al.* [2008]. Black stars are ocean bottom instruments, black inverted triangles are disposable sonobuoys, and white triangles are land seismometer stations. Black dashed lines are the 2-D wide-angle model lines. White dotted lines are seafloor-spreading anomalies 27n and 28n from *Collier et al.* [2008].

3.2. Receiver Functions

[13] Following the controlled source part of the experiment, the landstations were reconfigured and left to record teleseismic events for a further 12 months (February 2003 to February 2004 [*Hammond et al.*, 2005]). During this period a total of 34 earthquake events within an epicentral distance range of 40–90° were recorded. In addition we used 87 events recorded at the permanent station of MSEY on the main island of Mahé (station 04) between 1995 and 2005. Receiver functions were computed with an extended time multitaper method [*Helffrich*, 2006]. This method uses multitaper correlation in the deconvolution step, which prevents spectral leakage and down weights the noisy parts of the spectrum, an important consideration at island settings such as the Seychelles. The shear wave structure beneath each station to a depth of 200 km was then established by a combination of H-κ stacking [*Zhu and Kanamori*, 2000] and forward modeling [*Langston*, 1979; *Randall*, 1989]. The H-κ stacking indicated a V_p/V_s ratio of 1.78 for the crust, and so this value was used to convert the final receiver function derived S wave velocity models to P wave velocity models. Further details are given by J. O. S. Hammond et al. (Crust and upper mantle structure beneath the Seychelles: Architecture of a microcontinent, submitted to *Geophysical Journal International*, 2009).

4. Model Development

[14] A 2-D isotropic P wave velocity model for the crust and uppermost mantle was developed using a combination

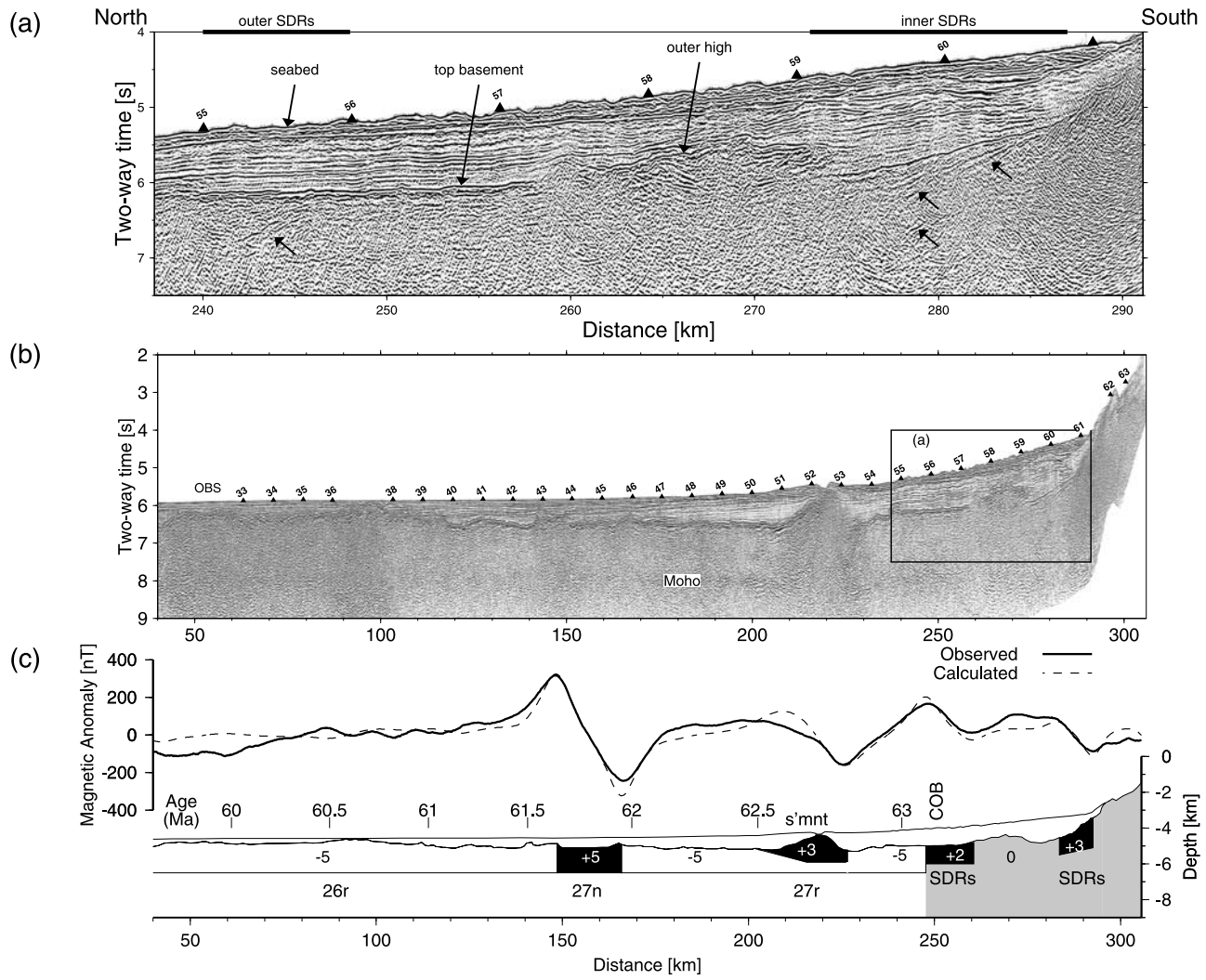

Figure 3. (a) Migrated stack of part of multichannel seismic line 9 showing seaward-dipping reflectors (marked with arrows). The data were collected with a 48 channel, 2.4 km long hydrophone streamer simultaneously with the shooting of the main wide angle. Seabed instruments are marked with numbered triangles. (b) Migrated stack of the whole of multichannel seismic line 9. The box marks the area of seaward dipping reflectors shown in detail in Figure 3a. The Moho reflection on a neighboring line can be seen in greater detail in Figure 9a. (c) Two-dimensional magnetic model of line 9 from *Collier et al.* [2008]. Blocks with natural remanent magnetization are shaded white/black according to reversed/normal polarity with the intensities given in A/m. The continental crust (shaded light gray) was assigned zero magnetic susceptibility, with all other blocks assigned a susceptibility of 0.04 SI. COB is the continent-ocean boundary. The two SDRs identified on the coincident reflection profile are modeled as weakly magnetized normal polarity bodies. Extending the 60 mm/a half spreading rate determined for anomalies 26r and 27n up to the COB implies that most of seafloor-spreading anomaly 27r is present, and so the SDRs are inferred to have erupted during chron 28n. The seamount at x = 220 km is modeled as a separate, normally magnetized body because dated samples recovered from a neighboring seamount (Darwin Hill, Figure 2) show them not to be contemporaneous with the underlying oceanic crust. The computed ages of the seafloor use the time scale of *Gradstein et al.* [2005].

of forward modeling and inversion using the ray theoretical programs FAST and RAYINVR [*Zelt and Smith*, 1992; *Zelt and Forsyth*, 1994; *Zelt and Barton*, 1998]. The former program inverts first arrival traveltimes only by ray tracing through a model with a uniform velocity mesh. The latter program inverts both first and secondary arrival traveltimes by ray tracing through a layered model defined at irregular, discrete depth and velocity nodes. RAYINVR input velocity models can be converted into FAST format velocity models to enable a rapid exploration of potential starting models.

[15] Our RAYINVR model has seven layers: water, sediments, upper crust, middle crust, lower crust, subcrustal body and mantle. The three crustal layers were included to enable sufficient vertical velocity gradient variation across the entire model to fit the data, but care was taken not to introduce strong velocity contrasts across them as no

Table 1. Model Results Summary[a]

Phase	Code	n	t_{unc} (s)	t_{RMS} (s)	χ^2
PcP	2.2	94	0.030	0.013	0.201
Ps	2.1	22	0.073	0.092	2.368
Pg1	3.1	486	0.043	0.050	1.334
Pg2	4.1	313	0.036	0.039	0.629
Pg3	5.1	785	0.041	0.039	0.868
PmP	5.2	207	0.060	0.055	0.845
Pn	6.3	261	0.048	0.028	0.329
Pu	7.1	44	0.088	0.118	2.197
PtP	5.2	39	0.065	0.074	0.711
PbP	6.2	21	0.147	0.222	2.035
All		2272		0.050	0.890

[a]Numbers of observations (n), average pick uncertainty (t_{unc}), average root mean square traveltime misfit (t_{RMS}), and normalized traveltime misfit (χ^2) for individual phases. If $\chi^2 = 1$, the model is a statistically perfect fit to the data given the assigned traveltime pick uncertainties. Code refers to the standard RAYINVR assignments, *nm*, where *n* is the deepest layer traversed by the ray and *m* is 1 for a turning ray, 2 for a reflection, and 3 for a refraction. PcP, basement reflection (including artificial zero offset picks made from the coincident reflection profile); Ps, sediment layer turning ray; Pg1–3, crustal layer turning rays; PmP, Moho reflection (including artificial zero offset picks made from the coincident reflection profile); Pn, mantle refraction; Pu, underplate turning rays; PtP, top underplate reflection; PbP, bottom underplate reflection.

intracrustal reflections were observed. The water layer properties were taken from the echo sounder and velocimeter probe measurements and were held fixed throughout the modeling. The initial sediment layer in the deep water part of the model was constructed from picks of the two-way time to top basement and semblance velocities from reflection line 9. We estimate that the sensitivity of the move out on the 2.4 km streamer data resolved the semblance velocity to within ±0.025 km/s throughout the <1 km thick sediment column [*Sansom*, 2006]. On the plateau, the initial sediment layer was constructed from picks to top basement from commercial reflection profiles (Figure 2, P. Joseph, personal communication, 2003).

[16] Owing to the relatively small size of the Seychelles microcontinent, recording turning waves from its lower crust presents some difficulties. We overcame this by supplementing the wide-angle data with landstation receiver functions and a historical east-west controlled source refraction line (profile 5210, Figure 4). The controlled source line, which crosses our transect 30 km south of the most southerly landstation on Mahé, (Figure 2) is unreversed but was collected with tethered sonobuoys [*Davies and Francis*, 1964]. The profile was originally interpreted with a line-intercept graphical method so we remodeled the original first-arrival traveltime picks using ray tracing. This work showed that the 5210 line provided good control on the seismic velocities down to a depth of 20 km from turning waves (Pg), but the structure of the lower crustal layer is determined by mantle refraction Pn alone and hence there is a trade-off between the velocity and thickness of this deepest crustal layer, and there is no information on the details of the lower crustal structure (Figure 4b). Overall the 5210 wide-angle model agrees well with the receiver function-derived profiles, and shows the Seychelles Plateau to have a typical continental velocity profile [*Christensen and Mooney*, 1995], with relatively high upper crustal velocities consistent with the exposure of granite on the Islands. The Mahé and Praslin Island receiver functions also showed the base of the crust to have a stepped seismic velocity structure.

[17] Once the water, sediment, and initial plateau structure had been defined, the first arrival picks were inverted with a range of minimum structure, geologically reasonable starting models with FAST. This provided a rapid means of determining a suitable starting model for the main modeling phase. The final model was then developed using RAYINVR, with a top-downward approach, and a combination of forward modeling and inversion until the normalized traveltime misfit (χ^2) for the entire data set fell to 1, and for each individual phase fell below 3 (Table 1). Throughout the traveltime inversion the velocity structure was checked for consistency against the coincident gravity, seismic reflection and magnetic profile (Figure 3) [*Collier et al.*, 2008]. For the gravity comparison, a two-dimensional model consisting of homogeneous density blocks was generated directly from the seismic velocity model. The shapes of the density blocks were not dictated by the velocity model layers but were computed from velocity contours chosen to characterize the lateral and vertical variation across the model. The predicted free-air gravity anomaly was then calculated using the two-dimensional line integral algorithm of *Talwani et al.* [1959]. A crossover error analysis of the gravity data collected in 2003 with other historical data from the region showed the likely error in the observed gravity to be ±5 mGal. The fit to the gravity was therefore deemed acceptable if it matched to within this uncertainty.

[18] The resolution of the final velocity model was estimated using the method described by *Zelt and Smith* [1992] that quantifies the relative ray coverage at model nodes. A measure of the uncertainty in the final model was gained by perturbing the velocity and depth nodes and recomputing the normalized traveltime misfit (χ^2). Changes were made to one layer at a time by adding or subtracting a fixed amount to either all the lower velocity or all the lower depth nodes. Once a complete set of perturbations had been made the results were plotted to ensure that the inverted model did indeed represent a minimum solution. The perturbed model χ^2 values were then compared to that of the final model using an F test, and errors assigned to the layer depths and velocities based on the models that were statistically different at the 95% confidence level.

5. Crustal Structure

[19] Selected wide-angle record sections and ray diagrams are shown in Figure 5, and the final velocity model in Figure 6. The model shows three distinct provinces: oceanic crust (model x = 50–255 km), characterized by thin crust and moderate crustal velocities (4.5–7.2 km/s); transitional crust (model x = 255–320 km), characterized by thickening crust and relatively high crustal velocities (5.0–7.3 km/s); and continental crust (model x = 255–460 km), characterized by thick crust and relatively low crustal velocities (5.5–6.8 km/s). The overall χ^2 fit of the model to 2272 traveltime picks is 0.89, and the RMS misfit just 50 ms (Table 1). The phases that are least well matched are the sediment turning ray (Ps), a deep subcrustal turning ray (Pu) and a deep reflection (PbP), all of which have relatively few total picks and the largest average pick uncertainties. All other phases have a χ^2 of less than 1.4.

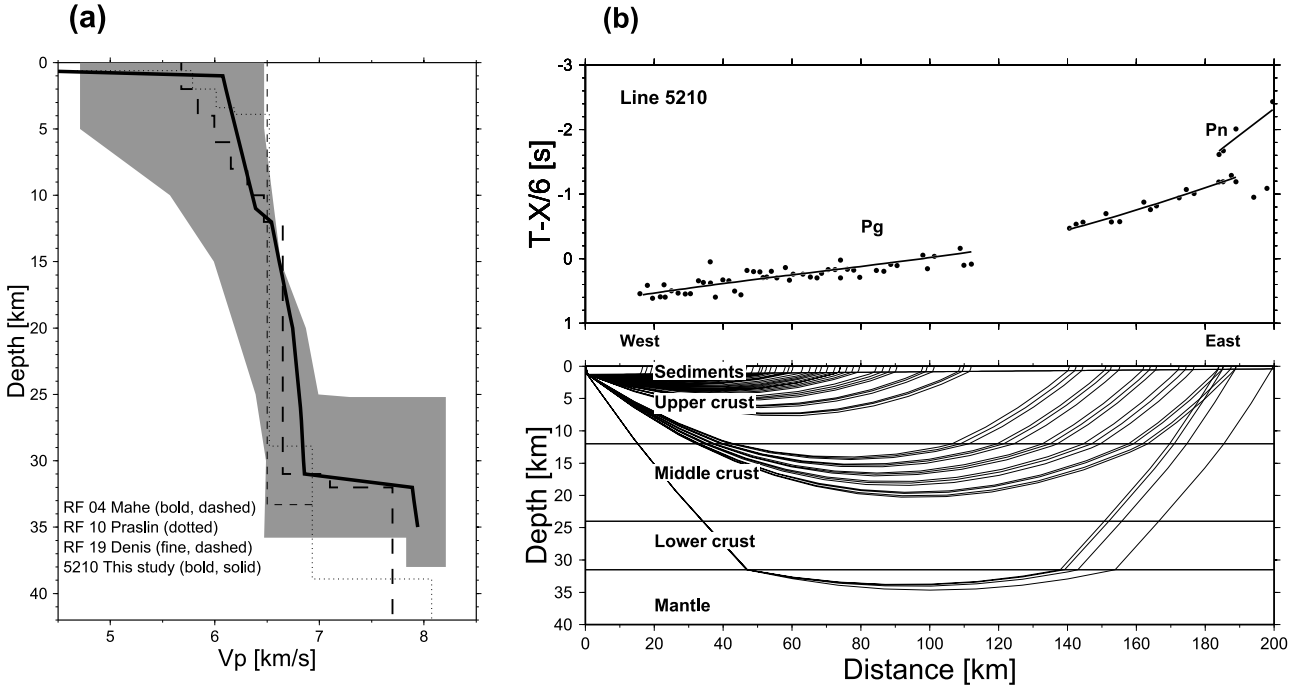

Figure 4. The Seychelles Plateau crustal structure. (a) Velocity-depth profiles obtained from receiver functions (RF; Hammond et al., submitted manuscript, 2009) and controlled source seismic refraction line 5210 (see Figure 1 for line location). The gray shading shows the range of extended continental crust profiles according to the global compilation of *Christensen and Mooney* [1995]. Of the three Seychelles receiver functions, the most reliable is that for Mahé (station 04, as it was calculated from the permanent station with the longest recording window) and the least reliable is that for Denis (station 19, as it is a low-lying coralline cay island with poorer signal-to-noise ratio than the granitic islands of Mahé or Praslin). This range of quality is reflected in the level of detail obtained in the velocity profiles. (b) Ray-traced forward modeling of the *Davies and Francis* [1964] original first arrival traveltime picks for line 5210. As the data are unreversed the model is assumed to be one-dimensional.

[20] The velocity structure of the oceanic crust is notably uniform throughout the length of the profile. The magnetic modeling showed that its age ranges between 63.1 and 60 Ma (Figure 3c) [*Collier et al.*, 2008]. This part of the seismic model is particularly well-resolved, with clear first arrival crustal turning waves (Pg), postcritical reflection from the Moho (PmP) and mantle refracted arrival (Pn) picks on each of the 8 km spaced seabed instruments (Figures 5a–5c). Note that the apparent low model resolution of the sediment layer (Figure 6b) is due to it having a close velocity and depth node spacing defined from the coincident multichannel data (constraints not included in the RAYINVR model resolution calculation). No sediment-turning rays (Ps) were identified on the seabed receivers from this part of the model and the wide-angle reflection from the basement (PcP) could only be recognized with confidence on about 25% of the instruments. The least well resolved crustal layer is the upper crust, as the first crustal rays to emerge from the direct wave turn just below the top basement. The resolution of all other parts of the model in this region is above the acceptable threshold of 0.5 [*Zelt*, 1999].

[21] The multichannel data show the sediments to thicken from 0.2 to 1 km from north to south across the oceanic crust part of the model. As a result of this change, all the crustal phases arrive later and Pg emerges from the direct wave with higher phase velocities, and hence turns slightly deeper in the crust on instruments to the south (e.g., compare Figure 5a and 5c). Otherwise the only difference in the record sections from OBS33 to OBS55 are small variations in the traveltime curves of Pg which correlate with basement topography. Velocity-depth profiles from three points along

Figure 5. Selected record sections with (top) picks (dots with error bars marking assigned uncertainty) and predicted arrivals (lines) overlain and (bottom) ray-traced model. Note that "offset" refers to the separation between the air gun source and the instrument (positive and negative values referring to shots south and north of the instrument respectively) and "distance" refers to the location along the wide-angle model. A reduction velocity of 8 km/s is used throughout. See text for explanation of phase names. The predicted direct arrival curve is included for the seabed sections for reference. Seabed multiples are labeled m. The seabed record sections are of the hydrophone component, and the land record sections are of the vertical geophone component. (a) OBS35, (b) OBS48, (c) OBH54, (d) OBH57, (e) OBH61, (f) OBH64, (g) landstation 19 (Denis Island), and (h) landstation 4 (Mahé Island).

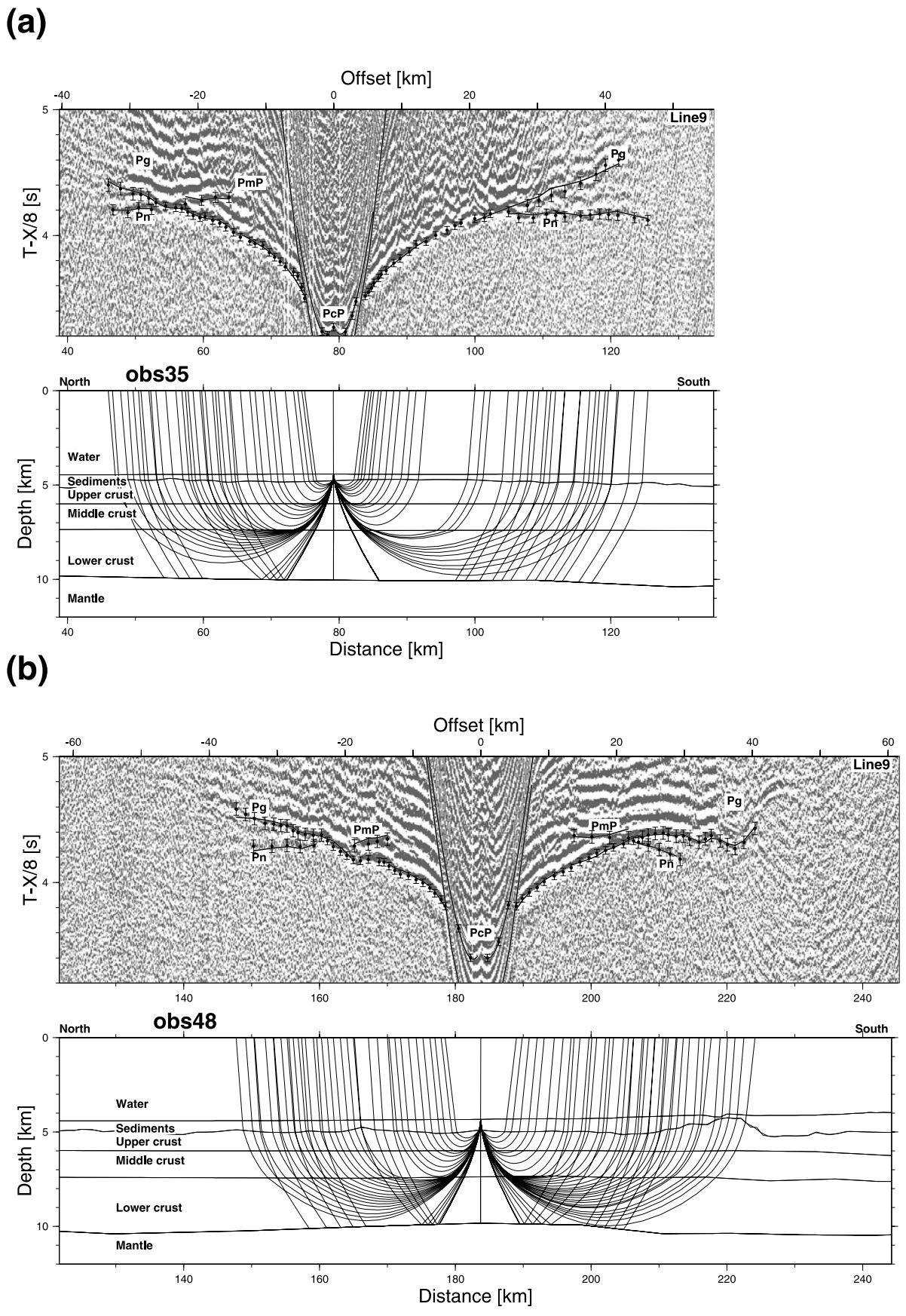
(a)
Offset [km]
Line9
Pg
PmP
Pn
PcP
T-X/8 [s]
obs35
North
South
Water
Sediments
Upper crust
Middle crust
Lower crust
Mantle
Depth [km]
Distance [km]
(b)
Offset [km]
Line9
Pg
PmP
Pn
PcP
T-X/8 [s]
obs48
North
South
Water
Sediments
Upper crust
Middle crust
Lower crust
Mantle
Depth [km]
Distance [km]

Figure 5

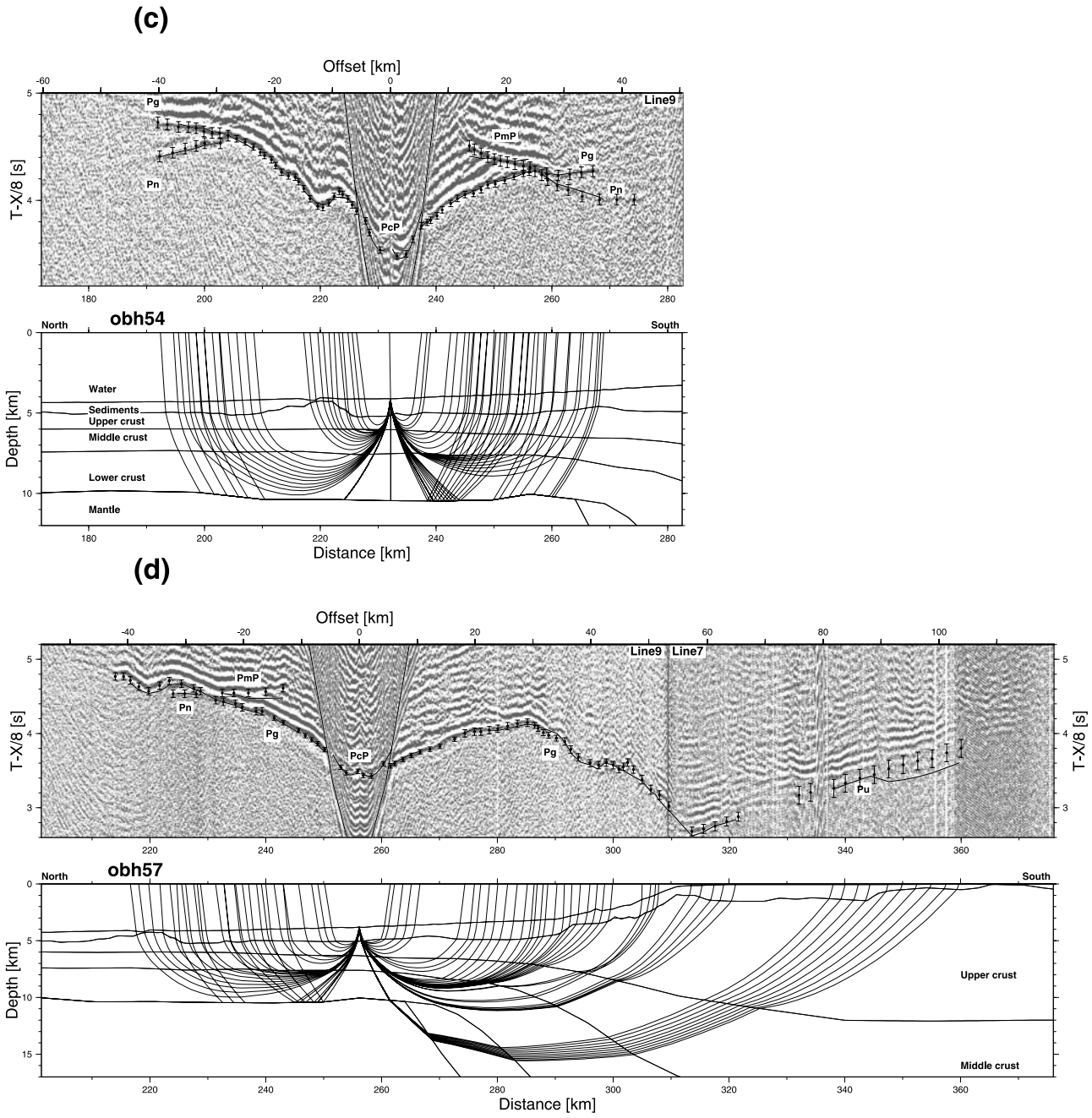

Figure 5. (continued)

the oceanic crust section are show in Figure 6c. The seismic velocities increase from about 4.5–7.2 km/s with depth. The uncertainty analysis conducted on the crustal layers showed an error of ±0.1 km/s in these velocities. The upper and middle crustal layers have a high velocity gradient of ~1.1/s, whereas the lower crustal layer (model layer 5) has a much smaller gradient of just 0.1/s. The seismic velocity structure obtained is typical of mature oceanic crust but it is significantly thinner [*White et al.*, 1992]. While the high velocity gradient upper crust has a similar thickness to that observed elsewhere, the lower gradient lower crust is thinner by about 2 km. The total crustal thickness averages just 5.2 ± 0.11 km along the entire length of this part of the model. Pn is seen on all the instruments here as a first arrival from about 25 km range, and shows the topmost oceanic mantle to have an average velocity of 8.24 km/s with an uncertainty of just ±0.03 km/s.

[22] South of OBS56, the seismic sections change character, with the maximum range of Pg increasing rapidly from 40 to more than 100 km, and both the mantle refraction (Pn) and Moho reflection (PmP), that are widely seen on instruments to the north, disappear. OBH57 is a good illustration of this change, with markedly different –north and –south record sections (Figure 5d). The change in the seismic records corresponds to the position of the outer seaward-dipping reflectors (SDRs) that are imaged on both the coincident reflection profile (Figure 3a) and on five of the six other parallel, normal incidence, seismic profiles

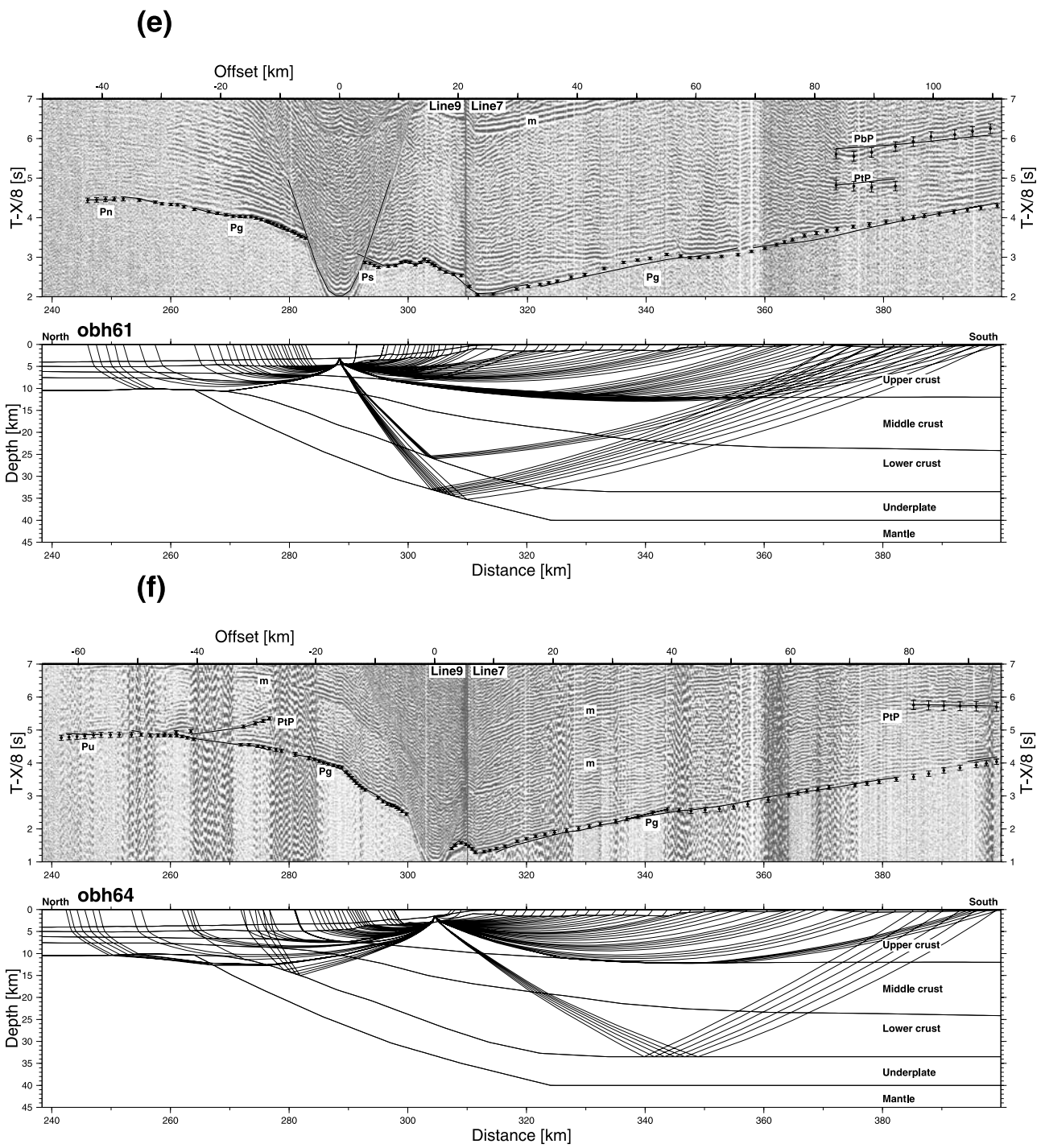

Figure 5. (continued)

(Figure 2). Work at other margins has shown that the outer SDRs usually coincide with the continent-ocean transition [*Planke et al.*, 2000]. This correlation appears to hold at the Seychelles margin also, and is consistent with our magnetic modeling which showed that a 200 nT positive anomaly could be best explained by the relatively abrupt juxtaposition of nonmagnetic continental crust and oceanic crust at this point (Figure 3c) [*Collier et al.*, 2008]. On several of the seismic profiles there is a clear basement high between the outer and inner SDRs. Similar features at other margins are usually referred to as the outer high and interpreted as due to the build up of hyaloclastic flows during explosive shallow water volcanism prior to the establishment of full seafloor spreading [*Planke et al.*, 2000]. Inner SDRs are usually interpreted as subaerial flows. This interpretation is supported here by geochemical results from a seamount that lies within the mapped inner SDRs (immediately west of line 12 and south of line 11 at 56° 12′E, 3° 34′S, water depth 3400 m, Figure 2). This seamount, which we interpret as a likely feeder to the surrounding SDRs, has a rare earth element

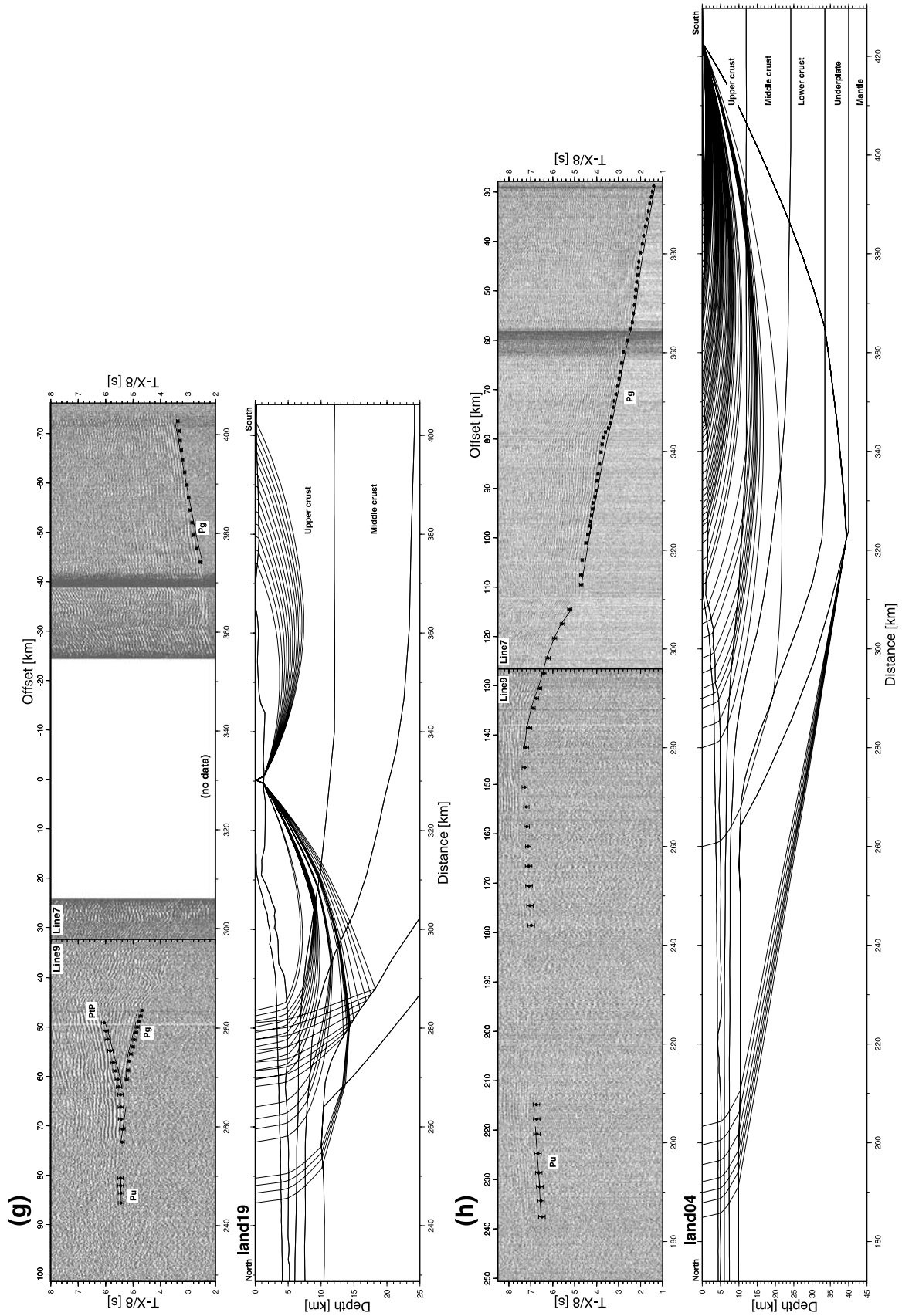

Figure 5. (continued)

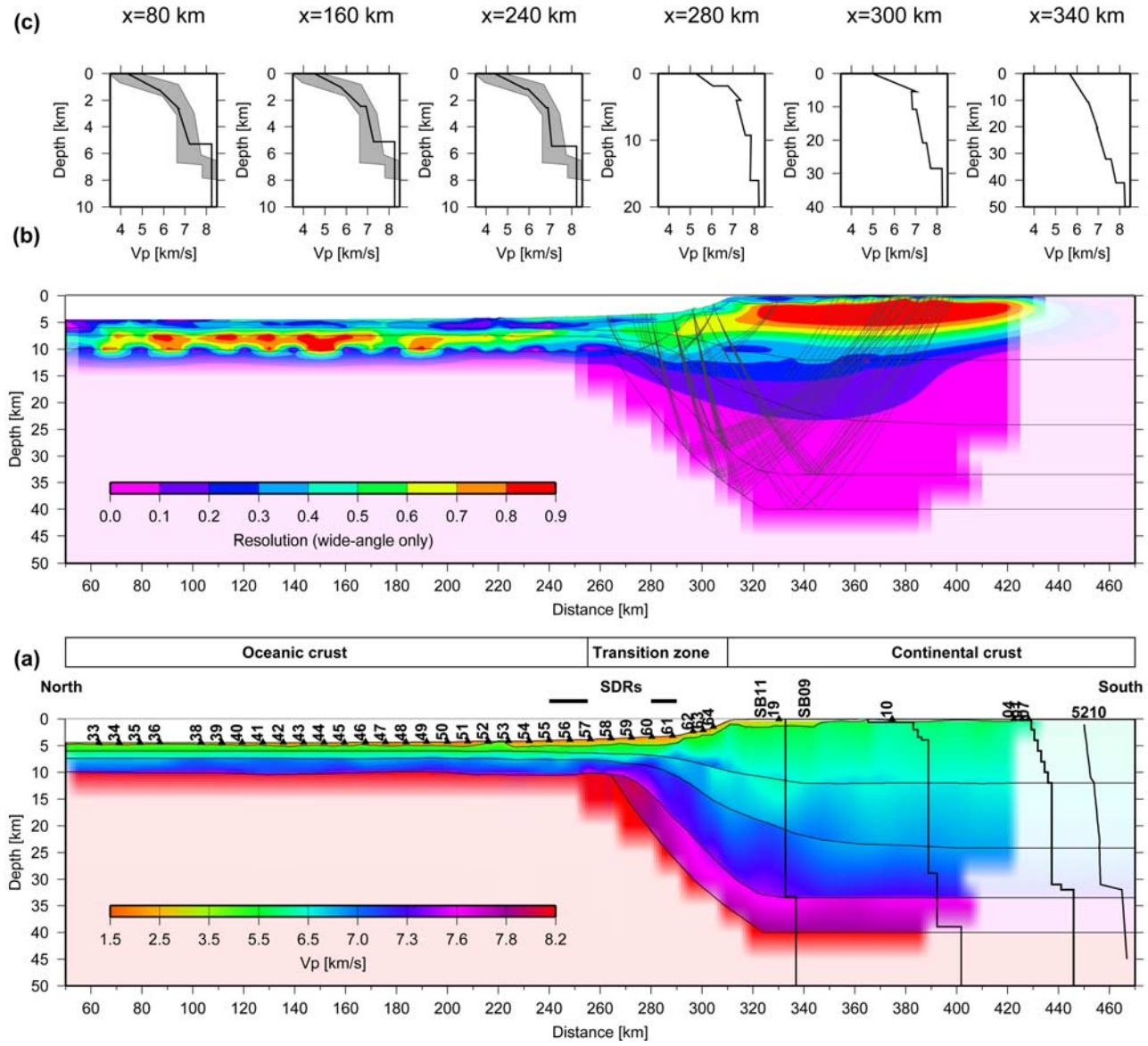

Figure 6. (a) Final *P* wave velocity model with model layer boundaries. Instrument positions are indicated with numbered triangles. The Mahé (station 04), Praslin (station 10), and Denis (station 19) receiver function velocity profiles and remodeled east-west controlled source profile 5210 are marked for reference. (b) Diagonal of the resolution matrix for the model velocity nodes shown as a contour plot. A value of 1 indicates full resolution, but for real data a value above 0.5 is considered acceptable [*Zelt*, 1999]. Note that there is a trade off between resolution and node spacing, which accounts for the apparent low resolution of the sediment layer which has dense node spacing defined from the seismic reflection data (and hence not taken into account in the calculation of the resolution). Also shown are the raypaths for the top (PtP) and bottom (PbP) underplate reflections from the transitional and continental parts of the model. (c) Velocity-depth profiles at various points across the model. The vertical scale is depth below top basement. The oceanic profiles (x = 800, 160, and 240 km) are compared to the envelope of values for 29–140 Ma old Pacific Ocean crust from *White et al.* [1992] (gray shading).

pattern which is consistent with subaerial eruption [*Collier et al.*, 2008]. On the basis of the seismic and magnetic analysis we therefore place the ocean-continent boundary at model x = 255 km, and refer to the model south of this point as the transition zone.

[23] The Pg first arrival times in the transition zone are strongly influenced by the rapidly shallowing seafloor that prevents the direct interpretation of their phase velocities. The traveltime inversion however shows that the velocities of the uppermost crust increase to above 5 km/s and the lowermost crust increase slightly to ~7.3 km/s in this region (Figure 6c). There appears to be a small velocity inversion at about 5 km below top basement. We interpret this velocity structure as due to the presence of the basaltic flows that form the SDRs and basaltic intrusions within the upper continental crust here. The semblance velocities

within the overlying sediments also increase to around 3.5 km/s in this region, and there are several particularly strong reflectors in the lower section that we interpret as basaltic sills. The largest offset wide-angle arrivals recorded in this region (Pu, Figures 5d, 5f, and 5g) indicate a seismic velocity of 7.6–7.8 km/s, significantly higher than expected for lower continental crust and significantly lower than the 8.24 km/s mantle velocity detected to the north. The most likely interpretation of this material, given its seismic properties and location is that it is mafic material intruded into and underplating the thinned lower continental crust. We model this material as a separate layer, which for ease of reference we have named underplate.

[24] South of OBS60, the record sections once again show wide-angle reflections from the lower crust (Figures 5e and 5f). Some of the record sections showed two wide-angle reflections, both with similar phase velocities but with a ~0.75 s difference in reduced traveltime (Figure 5e). Examination of the horizontal geophone components and forward ray tracing showed neither to be converted shear waves or multiples. We model these events as wide-angle reflections from the top (PtP) and bottom (PbP) of the intruded and underplated material detected by turning event Pu. Assuming the layer velocity to be between 7.6 and 7.8 km/s as indicated by Pu above 15 km depth, the underplate layer needs to be ~4 km thick to explain the observed reflection time difference between PtP and PbP. Further support for the extension of this underplate layer southward beneath the plateau comes from the Seychelles Island receiver functions. Despite the underplate being a somewhat subtle seismic feature (being relatively thin and with an intermediate seismic velocity between lower continental crust and mantle) its presence was detected beneath Praslin (station 10, 10 km thick) and Mahé (station 04, 1 km thick, Figure 4). Note that we do not think it significant that the underplate layer was not detected beneath Denis Island (station 19) as this receiver function had the poorest quality of those obtained and it also failed to resolve upper crustal structure seen on the other two stations.

[25] The offset and reduced time of PtP and PbP varies markedly across adjacent receivers indicating a rapid change in crustal thickness. The reflection traveltimes were reasonably well matched by an approximately linear interface dipping at 24° between model x = 270 and 320 km. Figure 6b shows the modeled PtP and PbP ray coverage and bounce points. The lack of deep turning rays resulted in the underplate layer being the least well resolved feature in the model, with a velocity uncertainty of +0.3/−0.35 km/s and thickness uncertainty of +0.7/−0.5 km. The overall shape of the crust however was independently supported by the need to match a prominent 120 mGal positive free air gravity anomaly on the outer Seychelles shelf (Figure 7). Systematic perturbations of the gravity model showed a tolerance of ±3 km in the depth of the lower continental crust layer (density 3.04 g/cm^3). The predicted gravity is not sensitive to the underplate layer itself (density 3.10 g/cm^3), for example removing it entirely changed the predicted gravity by less 5 mGal (the observational uncertainty). As a further external constraint on the shape of the lower crust, the receiver function recorded at Denis Island (x = 330 km) showed the crust to be 30 km thick, which is consistent with the PtP reflection seen on the most southerly OBH (Figure 5f). These observations indicate that the lateral distance from the ocean-continent boundary to full thickness continental crust is just 65 km.

[26] On the Seychelles Plateau itself, the wide-angle data further define the upper crustal structure, and show several 1–2 km thick, small sedimentary basins directly overlying >5.5 km/s basement. The velocity below top basement increases with a gentle gradient of just 0.05/s with depth.

6. Conjugate Margin Structure

[27] The conjugate Seychelles-Laxmi Ridge margin velocity models are shown together in Figure 8. The two profiles match well, and share a number of common features despite showing overall asymmetry, with the wide, complex Laxmi Ridge margin strongly contrasting with the much simpler and narrower Seychelles margin. Note that the 940 m vertical offset in the depth to basement on the northern margin can be entirely explained by an isostatic response to the load from the thick layer of Indus Fan sediment. We interpret the Laxmi Ridge itself as heavily intruded, thinned continental crust based on its seismic structure and magnetic properties [*Minshull et al.*, 2008; *Collier et al.*, 2008]. A set of seaward-dipping reflectors of comparable dimensions to those seen on the Seychelles side are imaged on its southern margin [*Collier et al.*, 2008]. Seaward of these SDRs, there is 5 km thick oceanic crust of chron 27r, which matches the age of that determined on the Seychelles side. The small (200 m) difference from the mean Seychelles oceanic crustal thickness is probably due to limitations of the velocity model in the north, where the velocity gradient at the top of the oceanic crust is poorly constrained because turning arrivals from this layer are obscured by earlier sedimentary arrivals. To the north of the Laxmi Ridge, the Gop Rift is interpreted as a failed rift underlain by oceanic crust. This interpretation is based on its seismic structure, presence of SDRs on its northern margin, and occurrence of strong magnetic anomalies symmetrically about a prominent basement ridge in the center of the rift that we interpret as an extinct spreading axis. Given that the Carlsberg Ridge has generated an unbroken set of magnetic anomalies from 27r to the present-day, the Gop Rift must have opened before the Seychelles rifted. Unfortunately, the Gop Rift is narrow and the magnetic anomaly sequence is too short to identify it uniquely [*Collier et al.*, 2008]. The mean thickness of the oceanic crust in the Gop Rift is 9 km, significantly thicker than that formed by the young Carlsberg ridge between the Laxmi Ridge and Seychelles. At the northern end of the profile, the crust is interpreted as continental crust marking the tapered edge of the Indian continental crust [*Malod et al.*, 1997]. The crust here is underlain by a high velocity subcrustal body which, like that beneath the Seychelles, is constrained by wide-angle reflections from its top and base. The body, which because of the imaging geometry is better resolved than in the Seychelles model, reaches a maximum thickness of ~12 km and has a velocity of 7.4 km/s. A second region with similar properties and hence also interpreted as underplate is imaged beneath the Laxmi Ridge itself, where it is constrained by both wide-angle reflections and turning waves. The robust detection of these underplate bodies beneath the northern conjugate margin lends support to our interpretation of PtP and PbP on the Seychelles side.

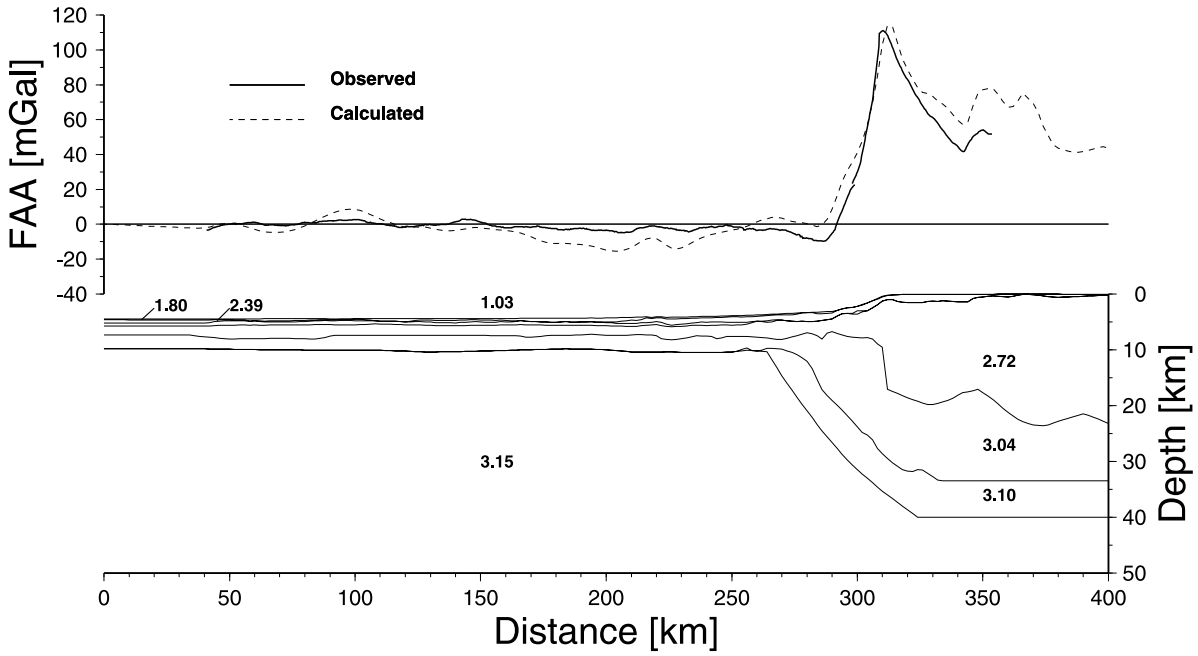

Figure 7. (bottom) Gravity model (densities in g/cm^3) and (top) calculated response. Crossover error analysis with historical ship tracks suggests an error of ±5 mGal on the observed free-air gravity anomaly. The model layer boundaries are defined directly from velocity contours of the final velocity model (Figure 6) without any adjustment. The sediments were defined by two blocks, with densities assigned according to their mean seismic velocity and the empirical velocity-density relationship of *Ludwig et al.* [1970]. The crust was defined by three blocks, with the densities assigned using the relationship $\rho = 0.989 + 0.289V_p$, from the linear solution to a global compilation of igneous and metamorphic rocks by *Christensen and Mooney* [1995]. The mantle was defined by a single block. We found that in order to model the long-wavelength (>200 km) gravity anomaly we needed to assign a relatively low density of 3.15 kg/m^3 to the mantle layer. We did not attempt to model the mantle structure in greater detail because of unknown contributions to the observed gravity deeper or outside the region constrained by the wide-angle data, but note that a low density in the lithospheric mantle beneath the plateau was predicted from the Mahé receiver function which showed it to have a *P* wave velocity of just 7.7 km/s (Figure 4a). Note that as the model is two-dimensional, short-wavelength (<50 km) features such as seamounts in deep water and sedimentary basins on the plateau will be overestimated if they are crossed by the profile and underestimated if they lie off-line.

The geometry of the underplate bodies suggest that they were formed when the Gop Rift opened. If they had formed during the Seychelles-Laxmi Ridge rift event they would be expected to be continuous across the Gop Rift [*Minshull et al.*, 2008]. Instead normal mantle velocities below normal lower oceanic crustal velocities were found in the Gop Rift. Significant underplating is also more consistent with the generation of thickened oceanic crust within the Gop Rift than the thin oceanic crust at the north Seychelles/south Laxmi Ridge margins.

7. Discussion

7.1. Comparison With Other Margins

7.1.1. Subaerial Volcanism

[28] Some of the first seaward-dipping reflectors were identified along the Indian Margin [*Hinz*, 1981] but since this early discovery the presence of extensive SDRs there has not been confirmed [*Gaedicke et al.*, 2002; *Krishna et al.*, 2006; *Minshull et al.*, 2008]. At the north Seychelles margin although SDRs were imaged on most of our multichannel seismic lines (see Figure 2 for their mapped distribution), they are not well expressed. Two sets of SDRs are present, an outer (oceanward) and inner (landward), the latter set being more widely and robustly imaged in our data set. Each set of SDRs is imaged for about 10 km along track with individual reflectors being traced laterally for up to 6 km (Figures 3a and 9a). The best-imaged set of reflectors is on line 13, where they reach a total thickness of 0.75 s TWT. In comparison, at the Edoras Bank margin of the North Atlantic, which at ~1100 km from the Iceland plume should be comparable with the Seychelles margin, the SDRs extend laterally for 70 km and are 2 s TWT thick (Figure 9) [*Barton and White*, 1997]. Although the sediments are thicker at the Seychelles than at the Edoras margin, given the widespread imaging of Moho beneath the SDRs in our data, we do not consider that this difference is a result of poor seismic energy penetration. While care needs to be taken when drawing conclusions from SDRs as it has been shown that seaward-dipping lava formations may exist without having a seismic expression [*Eldholm et al.*, 1986; *Planke and Eldholm*, 1994; *Planke et al.*, 2000], the poor development of SDRs at the Seychelles margin is consistent with modest subaerial/

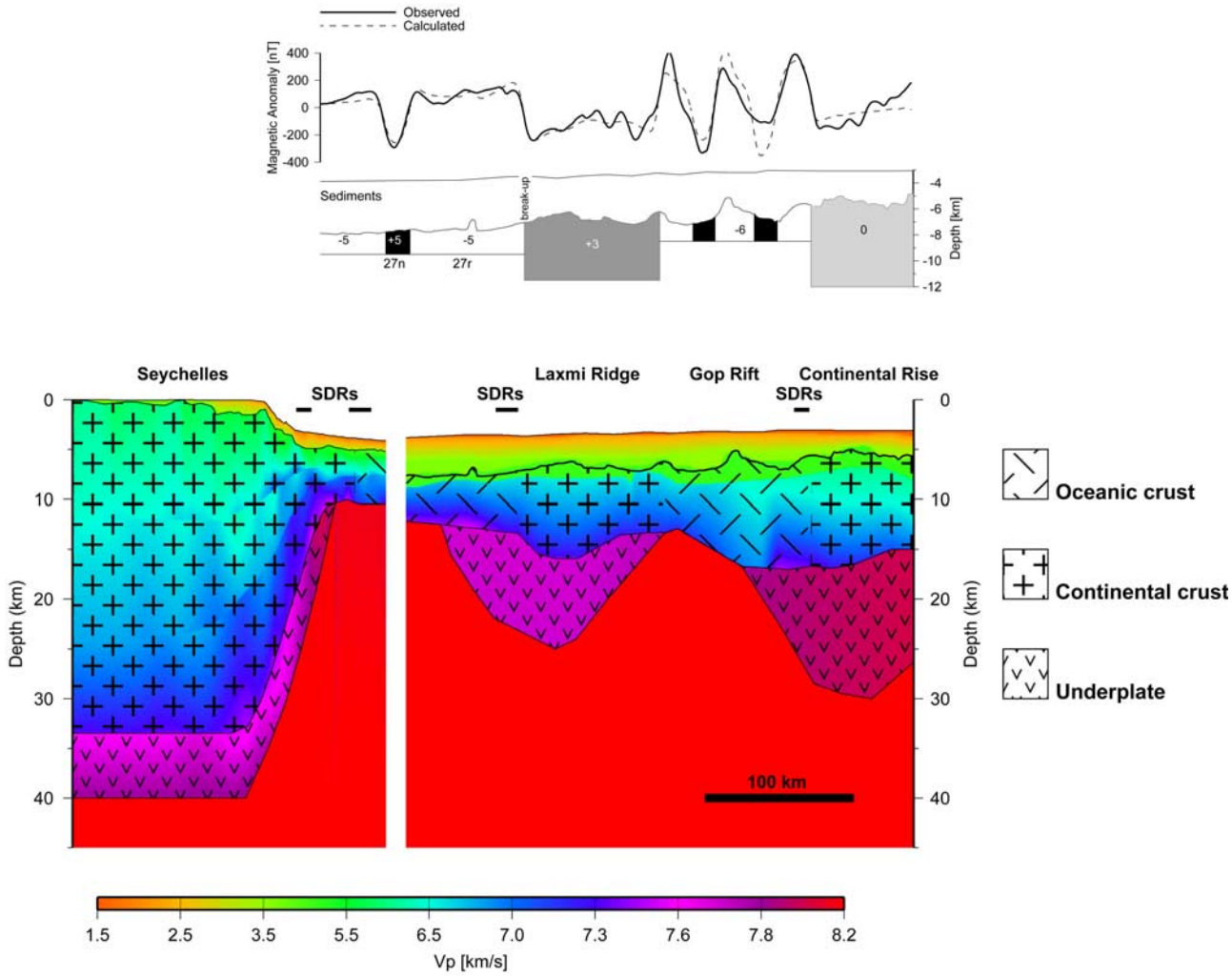

Figure 8. (bottom) Seismic structure of the conjugate Seychelles-Laxmi Ridge margins, with (top) magnetic model for the Laxmi Ridge margin [*Collier et al.*, 2008]. Both margins were surveyed during a single cruise using the same experimental techniques. The Laxmi Ridge margin data were modeled independently but using the same methods as described here [*Lane*, 2006; *Minshull et al.*, 2008].

shallow marine volcanism that would be expected to precede the generation of 5.2 km thick oceanic crust.

[29] It is also significant that we found no evidence for a thick flood basalt sequence on top of the northern Seychelles Plateau. In western India the upper continental crust is characterized by a velocity inversion with an up to 3 km layer of 4.8–5.1 km/s basalts overlying 1–2 km of Mesozoic sediments with velocities of 3.1–3.2 km/s [*Reddy*, 2005]. While we have evidence for a small velocity inversion on the slope, there is no evidence for one on the plateau itself. Instead, on the plateau, a number of isolated, 1–2 km thick, small sedimentary basins with velocities of 2.5–3.5 km/s directly overly >5.5 km/s basement. The upper continental crustal structure is particularly well resolved in our model, and so a thick basaltic layer is certainly missing. This observation is important as the entire northern Mascarene Plateau from the Saya de Malha Bank up to and including most or all of the Seychelles Plateau (the region between the labels "MP" and "SP" in Figure 1c, an area of 2.5×10^5 km^2) has been previously included as part of the Deccan province by both *White and McKenzie* [1989] and *Coffin and Eldholm* [1994]. We consider it unlikely that a significant part of the northern Mascarene Ridge south of the Seychelles continental block could have been formed during the main phase of Deccan activity without significantly more offshore magmatism being produced during continental breakup. The spatial extent of the Deccan flood basalt province is therefore smaller than previously thought.

7.1.2. Initial Oceanic Crustal and Margin Width

[30] In order to investigate the significance of the initial oceanic crustal thickness generated at the Seychelles margin we made a compilation of observations at other margins (Table 2). We restricted our analysis to studies in which the crustal structure was constrained by modern wide-angle seismic methods, except in the South Atlantic where in order to achieve a reasonable geographical coverage we included one study that relied on gravity modeling of multichannel seismic data [*Mohriak et al.*, 1998] and one that relied on sonobuoys [*Chang et al.*, 1992]. For areas such as offshore Norway, where there were many suitable surveys, only one representative survey per region was chosen. We included the Gulf of California margins in the compilation but we

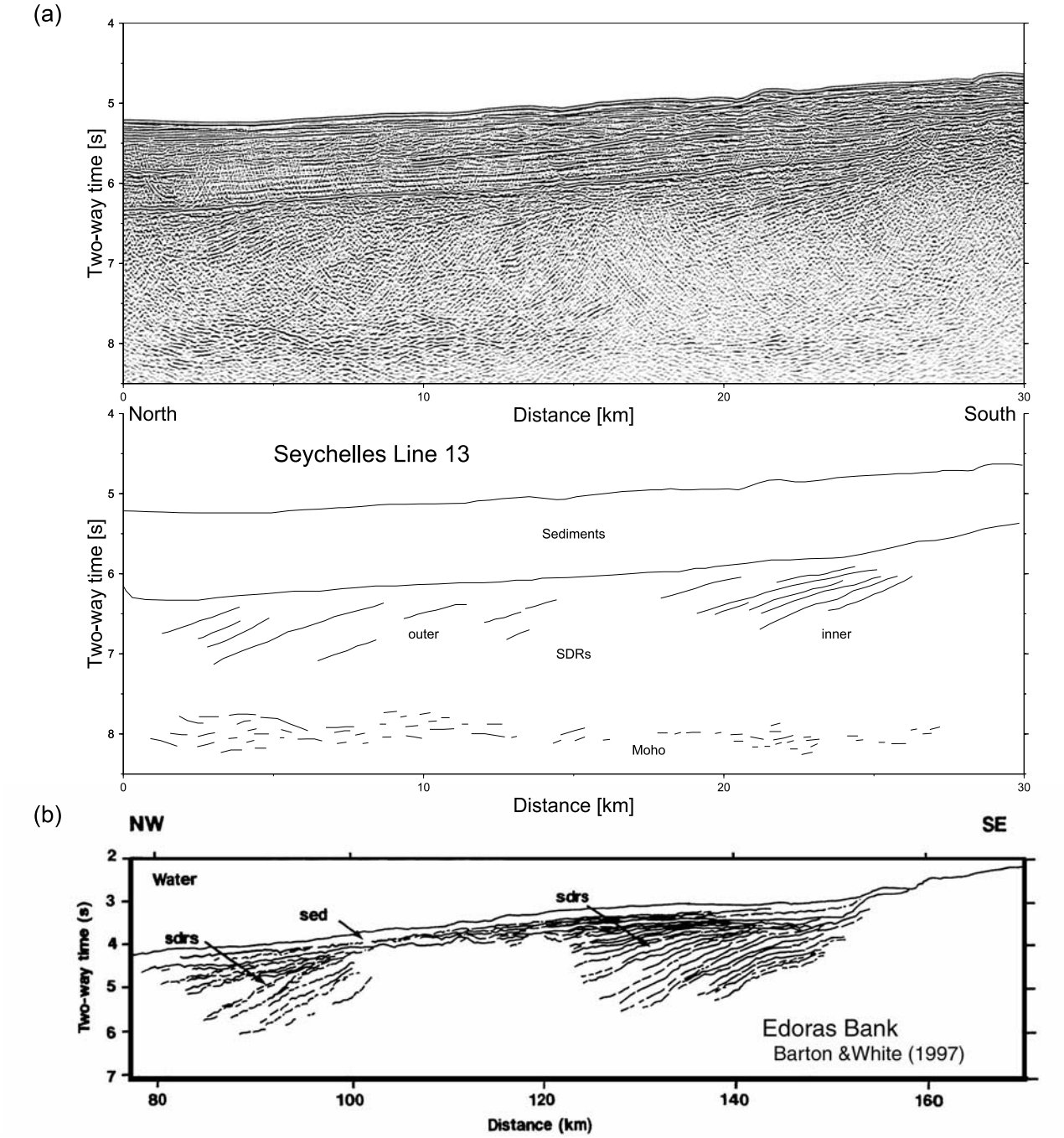

Figure 9. (a) Multichannel seismic line 13 and line drawing showing the best-imaged seaward-dipping reflector package from the north Seychelles margin. (b) Line drawing of SDRs at the north Atlantic Edoras Bank margin from *Barton and White* [1997]. Note the different plot scales and much more extensive SDR development at the distal North Atlantic margin.

note that these three profiles show unusually rapid along strike changes in structure, which have been attributed to the local setting [*Lizarralde et al.*, 2007]. The geographic distribution of our selected profiles is shown in Figure 10. The thickness of earliest oceanic crust was measured from the original published velocity models at the point immediately seaward of the outer SDRs in the case of volcanic margins or immediately seaward of serpentinized mantle in the case of nonvolcanic margins. For profiles where neither of these features was present, the thickness was measured on the oldest unequivocal oceanic crust as indicated by the seismic velocity structure, reflective nature of the top basement and magnetics. Care was taken to ensure as consistent a set of measurement points as possible, which required some reinterpretation of crustal type compared to that given by the original authors in a few cases. In the case of the North and South Atlantic profiles, we then computed their distance from the Iceland and Tristan da Cunha hot spots respectively at

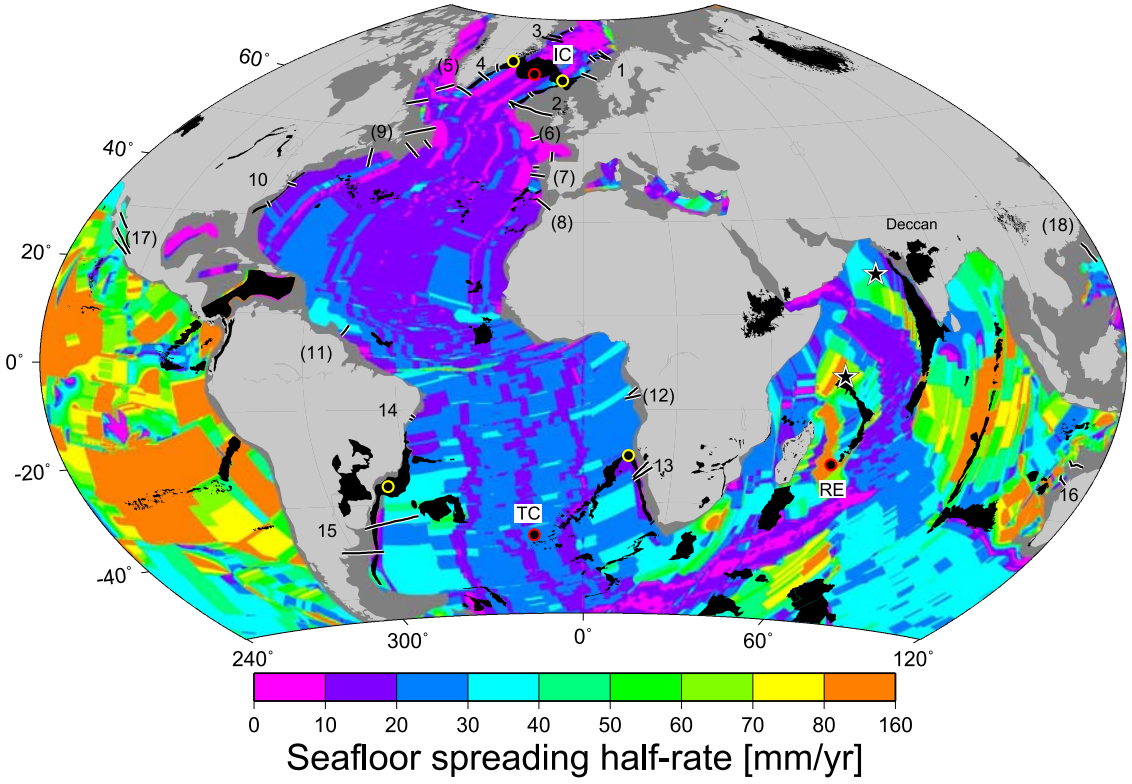

Figure 10. Locations of selected previous passive margin seismic experiments detailed in Table 2. Individual seismic profiles are marked with black lines, with reference numbers in brackets indicating margins defined in Table 2 as "nonvolcanic" or "intermediate." The stars mark the Seychelles-Laxmi Ridge study areas. Large igneous provinces from *Coffin and Eldholm* [1994] are shaded black and hot spots linked with continental breakup and plume tail offshore ridges discussed in the text are labeled IC, Iceland; TC, Tristan da Cunha; RE, Réunion. The yellow circles with black centers mark the assumed positions of the Iceland and Tristan da Cunha hot spots at the time of continental breakup used to calculate the plume offset distances in Table 2. Seafloor-spreading rates are from *Muller et al.* [2008].

the time of continental breakup inferred from the positions of their associated aseismic ridges (Figure 10). We chose to exclude the nonvolcanic Labrador Sea margins [*Chian and Louden*, 1994; *Chian et al.*, 1995] from the North Atlantic province as it is commonly argued that they rifted before the Iceland hot spot initiated [*White and McKenzie*, 1989]. However, we note that the age of the oldest oceanic crust here is disputed, and other authors consider that the margins formed within ~700 km of the starting Iceland plume [*Nielsen et al.*, 2002].

[31] Our compilation showed that the 5.2 km thick oceanic crust formed at the north Seychelles margin is indisputably thin. Indeed, somewhat surprisingly given the tectonic setting of the Seychelles margin, the oceanic crust here is even thinner than many of the nonvolcanic margins listed in Table 2, that have an average of 5.8 ± 1.0 km (excluding the Moroccan margin where oceanic crust may have been thickened by later volcanism [*Contrucci et al.*, 2004a]). Next, we plotted selected margin parameters in order to test relationships predicted by current rift-magmatism models. The first relationship we investigated was oceanic crustal thickness versus distance from hot spot center (Figure 11a). The North Atlantic margins, which have been particularly well studied with many high-quality profiles, show a clear, approximately linear reduction in the thickness of the earliest-formed oceanic crust with distance from the center of the Greenland-Iceland-Faeroe Ridge. This pattern has been previously interpreted by *Barton and White* [1997] as being due to a reduction in the mantle thermal anomaly with distance away from the Iceland plume at the time of rifting. At distances away from the Iceland plume similar to those of our Seychelles profile from the Deccan hot spot, the oceanic crustal thickness found along the North Atlantic margins is more than twice as thick. The relationship between distance from hot spot center and thickness of the first formed oceanic crust in the South Atlantic is less clear, perhaps in part due to the smaller number and poorer quality of observations. However, here too there appears to be an approximately linear relationship, and the oceanic crust at similar distances to the Seychelles study area is one and a half times thicker.

[32] The second relationship we investigated was oceanic crustal thickness versus margin width (Figure 11b). We define margin width as the distance from the point at which we measured the initial oceanic crustal thickness to the position of full thickness continental crust (itself defined as a thickness of more than 25 km unless the crustal model suggested a smaller value was acceptable). While there is considerable scatter in the data, our new compilation confirms the tendency for the thickness of the first-formed oceanic crust to reduce with increasing margin width, as previously noted

Table 2. Compilation of Results From Other Studies of Continental Rifted Margins[a]

Province	Reference Number	Margin Name	Reference	Wide-Angle Profile	Data[b]	Type	Longitude	Latitude	Distance to Hot Spot Center (km)	Earliest Oceanic Crust Thickness (km)	Margin Width[c] (km)	Onset Seafloor Half Spreading Rate (mm/a)
	Star	Seychelles	This study	Line 9 + 7	OBS	int	56	−3	1000	5.2	65	60.0
North Atlantic	1a	Lofoten	*Goldschmidt-Rokita et al.* [1994]	LM 1A	OBS	v	9.5	69.1	1076	8.7	>120	8.4
	1b	Lofoten (south)	*Mjelde et al.* [1992]	Line 3	OBS	v	8.2	68.8	1014	11.8	135	9.7
	1c	Voring	*Mjelde et al.* [2005]	Obs99	OBS	v	3.8	68.2	834	17.4	>105	9.4
	1d	Møre	*Olafsson et al.* [1992]	MVM 1	ESP	v	0.1	64.1	444	18.1	340	12.6
	2a	Hatton Bank	*Fowler et al.* [1989]	N18	ESP	v	−19.3	59.4	697	11.3	100	8.1
	2b	Hatton Bank (south)	*Vogt et al.* [1998]	RAPIDS	OBS	v	−23.4	56.7	1072	14.2	400	14.3
	2c	Edoras	*Barton and White* [1997]	Cam77	OBS	v	−24.0	56.6	1109	11.5	>80	14.3
	3a	NE Greenland	*Mutter and Zehnder* [1988]	COP 39,40	ESP	v	−7.2	75.5	1264	7.1	>70	7.9
	3c	NE Greenland	*Mutter and Zehnder* [1988]	COP 46	ESP	v	−14.9	73.8	976	7.2	>55	8.3
	3d	NE Greenland	*Mutter and Zehnder* [1988]	COP 61	ESP	v	−16.1	72.9	880	12.9	>115	8.7
	3e	NE Greenland	*Voss and Jokat* [2007]	400	OBS	v	−16.7	73.7	923	11.4	200	8.3
	3f	NE Greenland	*Voss and Jokat* [2007]	500	OBS	v	−18.0	72.9	832	7.0	260	8.3
	4a	SE Greenland	*Holbrook et al.* [2001]	Sigma II	OBS	v	−35.9	64.7	321	28.0	160	12.7
	4b	SE Greenland	*Holbrook et al.* [2001]	Sigma III	OBS	v	−39.0	62.7	591	17.0	120	14.8
	4c	SE Greenland	*Holbrook et al.* [2001]	Sigma IV	OBS	v	−42.2	59.1	1022	14.5	100	13.3
	5a	SW Greenland	*Chian and Louden* [1994]	88R2	OBS	nv	−50.0	60.0	n/a?	6.7	150	6.2
	5b	Labrador	*Chian et al.* [1995]	90R1	OBS	nv	−56.2	56.2	n/a?	5.5	270	6.3
Central Atlantic	6a	Goban Spur	*Bullock and Minshull* [2005]	WAM	OBS	nv	−14.5	48.5	n/a	5.1	>100	4.0
	7b	Biscay	*Fernéndez-Viejo et al.* [1998]	IAM 12	Land	int	−8.8	44.5	n/a	7.0	60	5.5
	7c	Galicia Bank	*Whitmarsh et al.* [1996]	Line 6	OBS	nv	−13.0	42.1	n/a	7.3	>150	10.3
	7d	Iberia	*Dean et al.* [2000]	IAM 9	OBS	nv	−13.0	40.5	n/a	5.7	250	7.0
	8a	Moroccan	*Contrucci et al.* [2004a]	Profile 4	OBS	nv	−10.5	34.3	n/a	7.9[d]	220	11.8
	9a	Orphan Basin	*Chian et al.* [2001]	86−6(8)	OBS	nv	−44.5	50.3	n/a	4.6	235	3.8
	9b	Flemish Cap	*Funck et al.* [2003]	Screech 1	OBS	nv	−43.5	46.4	n/a	6.5	140	13.7
	9c	Grand Banks	*Lau et al.* [2006]	Screech 3	OBS	nv	−46.0	44.0	n/a	6.2	280	13.3
	9d	Nova Scotia	*Funck et al.* [2004]	Smart 1	OBS	nv	−58.0	42.7	n/a	3.9	320	15.8
	10a	Baltimore Trough	*Holbrook et al.* [1994a]	EDGE 801	OBS	v	−74.0	36.4	n/a?	11.1	125	27.1
	10b	Carolina Trough	*Holbrook et al.* [1994b]	BA 6	OBS	v	−76.5	31.7	n/a?	10.3	60	29.1
	11a	Guiana	*Greenroyd et al.* [2007]	Profile A	OBS	int	−51.0	6.0	n/a	4.8	125	20.6
South Atlantic	12a	Congo	*Contrucci et al.* [2004b]	Profile 14	OBS	int	10.2	−6.4	1487	6.4	>170	29.7
	12b	Angola	*Contrucci et al.* [2004b]	Profile 7 + 11	OBS	int	10.5	−7.4	1385	6.4	>135	28.7
	13a	Namibia	*Bauer et al.* [2000]	Transect 1	OBS	v	11.9	−23.8	489	9.4	230	13.6
	13b	Namibia (south)	*Bauer et al.* [2000]	Transect 2	OBS	v	11.9	−24.7	580	6.8	170	13.2
	14a	Brazilian	*Mohriak et al.* [1998]	Profile A	MCS + gravity	v	−36.3	−11.6	1850	7.2	>70	19.4
	14b	Brazilian	*Mohriak et al.* [1998]	Profile C	MCS + gravity	v	−36.8	−12.1	1773	7.4	35	21.0
	15a	Uruguay	*Chang et al.* [1992]	Profile B	Sonobouys	v	−50.4	−34.3	1047	7.8	314	7.2
	15b	Argentine	*Franke et al.* [2006]	BGR98−01	OBH	v	−53.3	−40.0	1729	7.7	125	11.4

Table 2. (continued)

Province	Reference Number	Margin Name	Reference	Wide-Angle Profile	Data[b]	Type	Longitude	Latitude	Distance to Hot Spot Center (km)	Earliest Oceanic Crust Thickness (km)	Margin Width[c] (km)	Onset Seafloor Half Spreading Rate (mm/a)
West Australia	16a	Cuvier	*Hopper et al.* [1992]	Line 670	ESP	v	111.6	−22.2	n/a	10.0	65	23.2
	16b	Exmouth Plateau	*Mutter and Larson* [1989]	Line 652	ESP	int	111.7	−18.7	n/a	6.0	200	34.8
West America	17a	Gulf of California	*Lizarralde et al.* [2007]	Segment G	OBS	int	−111.6	27.4	n/a	8.0	150	47.3
	17b	Gulf of California	*Lizarralde et al.* [2007]	Segment A	OBS	int	−109.0	22.8	n/a	6.8	300	49.3
	17c	Gulf of California	*Lizarralde et al.* [2007]	Segment C	OBS	int	−109.1	24.0	n/a	5.0	100	46.3
SE Asia	18a	China	*Nissen et al.* [1995]	Eastern	ESP	int	118.6	18.6	n/a	5.5	300	36.9

[a]Compilation of results from other studies of continental rifted margins. See Figure 10 for survey locations. The margins are classified according to features within the continent-ocean transition: v, volcanic if they display thick SDRs and underplate; nv, nonvolcanic if they display tilted fault blocks and serpentinized mantle; int, intermediate if they do not readily fall into the other two categories. The distance to hot spot center in the North Atlantic and South Atlantic are measured from the point on the profile of the first oceanic crust to the center of the oldest parts of the Greenland-Iceland-Faeroe Ridge, Rio Grande Rise, and Walvis Ridge (as marked with the yellow circles in Figure 10). Where full thickness continental crust was not achieved on the wide-angle profile, the measured margin width is marked with a > symbol. The onset seafloor-spreading rate was extracted from the digital grid of *Muller et al.* [2008] (Figure 10). In a few cases we needed to use a rate from up to 20 km oceanward of our actual oceanic crust thickness measurement point. We rejected some seismic profiles from our compilation at this stage (for example around Antarctica) if an associated seafloor-spreading rate was not available.

[b]ESP, expanding spread profile; MCS, multichannel seismic.

[c]A > symbol means that full thickness continental crust is not achieved on the profile (defined as a thickness of more than 25 km unless data suggests a smaller value was acceptable) and so the measured width is a minimum bound estimate.

[d]This, overprinted with late Cenozoic volcanism and the original oceanic crust, may have been thinner.

by the authors of the small-scale convection models [*Mutter et al.*, 1988]. However, as can be seen from the compilation the Seychelles margin is relatively narrow and therefore these models would predict it to have thickened oceanic crust, although possibly active convection was damped by the wide Laxmi conjugate margin. In addition to crustal thickness, the seismic velocity of the oceanic crust formed along continental margins may also be diagnostic of the rift dynamics [*Kelemen and Holbrook*, 1995; *Holbrook et al.*, 2001]. According to these workers, active convection is expected to generate oceanic crust with a lower seismic velocity than that generated by passive melting under elevated mantle temperature because melting occurs shallower and so produces melts poorer in MgO and richer in SiO_2. Following the approach detailed by *Holbrook et al.* [2001], we calculate a mean oceanic crustal velocity of 6.93 ± 0.02 km/s for the north Seychelles margin. According to their model (Figure 11c), this seismic velocity coupled with a mean thickness of 5.2 ± 0.1 km, indicates that the crust formed by passive upwelling only (i.e., no small-scale convection) with a mantle potential temperature of 1275°C (i.e., slightly cooler than "normal" 1300°C mantle). Results for the distal Greenland margins (dots labeled 4b and 4c, Figure 11c) also indicate a lack of active upwelling but the predicted mantle temperatures are 100°C hotter. We note that the fast spreading (65 mm/a) Seychelles oceanic crust has very similar properties to the fast spreading East Pacific Rise at 17°S (diamond labeled epr, Figure 11c). On the basis of this result we will not discuss active upwelling models further.

7.2. Factors Influencing Magmatism During Continental Breakup

[33] Our observations at the Seychelles margin are at odds with the predictions of the plume head model of melt generation during continental breakup. In this model the voluminous magmatism observed at volcanic continental margins is due to the transient high temperatures and flow rates generated as a new plume impacts the base of the lithosphere [*White and McKenzie*, 1989; *White*, 1992b]. Several workers have noted that the 2000–2500 km extent of the volcanic margins that border the north Atlantic is comparable with the theoretical predictions of a diameter of a flattened circular plume head, and cited this observation as support for this model [*Campbell*, 2007]. If this scenario is correct, then we would need to invoke a smaller/colder plume head in the Deccan case to match our new seismic observations. However, we note that the volume of the onshore Deccan is estimated to be very similar to that of both the onshore North Atlantic Tertiary Volcanic and the South American Parana provinces (extrusive components 1.5×10^6 km^3, 1.8×10^6 km^3, and $>1.5 \times 10^6$ km^3, respectively [*Coffin and Eldholm*, 1994; *White and McKenzie*, 1995]), and so it seems more reasonable to infer that they originated from mantle plumes of similar sizes and temperatures. Indeed, theoretical work shows that mantle plume size and temperature is largely dictated by the height of ascent, so if the Iceland, Tristan de Cunha and Reunion plumes all formed from the same depth (be it the base of the mantle or base of the upper mantle) they should have had similar properties [*Campbell*, 2007]. We conclude that the symmetrical flattened plume head model is not compatible with our observations at the north Seychelles margin.

[34] Several workers have previously emphasized that the lateral flow of plume material beneath the lithosphere may not be a simple radial process, such that the distribution of hot material beneath a region experiencing plume impact is case specific. If this is correct then it would not be appropriate to directly compare the extent of volcanic rifted margins to the dimensions of the flattened, circular plume head [*Sleep*, 1997]. Lateral flow could also be important for non-plume sources for the flood basalt generation, such as edge-driven convection, where a central zone of upwelling mantle flows laterally beneath the surrounding lithosphere. In the plume case, the variation in the spatial distribution of the thermal anomaly might be exacerbated if, rather than having an axisymmetric ("mushroom head") geometry, the arriving plume head had a more complicated shape, such as an initial three-armed form, as has been predicted in some numerical models [e.g., *Houseman*, 1990] and it does not have a long incubation period beneath the lithosphere in which to thermally equilibrate prior to rifting. Hence it may not be appropriate to expect all margins formed at similar lateral distances from the center of a similarly sized plume to display common magmatic characteristics. *Nielsen et al.* [2002] applied this idea to explain the formation of the nonvolcanic margins of the Labrador Sea (which they believe formed within the North Atlantic province) as being due to the flow of Iceland plume material being blocked by the thick Greenland craton. This idea, however, is not so readily applied in the Seychelles case, as it could be argued that the plume material would be expected to have flowed upslope from the Indian craton toward the Seychelles, given that the lithosphere here was probably already thinned when Greater India split from Madagascar ~20 Ma earlier. Perhaps when the Gop Rift opened it exhausted the hot asthenospheric layer bought by the plume. Alternatively, in the Iceland case hot material could have been preferentially fed into the North Atlantic margins because the developing

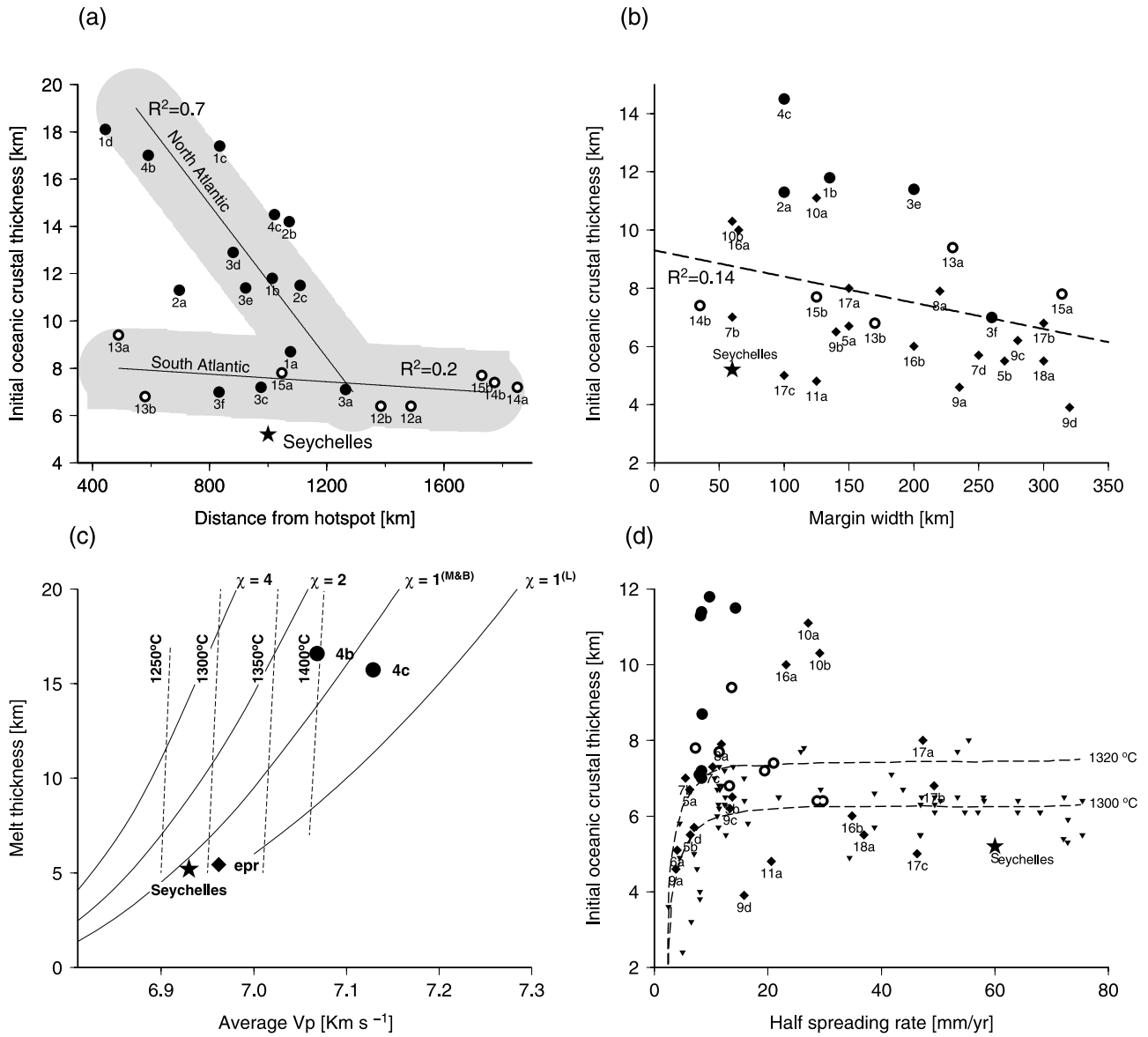

Figure 11

rift intersected the central stem of the new plume. In the case of the Seychelles, the margin is offset from the Deccan center and the "plume tail" Chagos-Laccadive Ridge is not orthogonal to the continental margins (Figure 1a). It has also been suggested that the South Atlantic margins did not intersect the plume axis either [*Peate et al.*, 1990; *Harry and Sawyer*, 1992], and so perhaps this is also the explanation for the lower degree of magmatism observed along these margins compared to those in the North Atlantic.

[35] An intriguing alternative possibility is that the difference in the structure of the Seychelles and distal Atlantic margins is related to differences in efficiency of melt extraction at varying plate divergence rates. In order to investigate this idea, we plotted the thickness of the initial oceanic crust against initial seafloor-spreading rate for each of our compiled continental margins together with other measurements of oceanic crust thickness made away from continental margins (Figure 11d). In this diagram, the relatively high initial seafloor-spreading rate of the Seychelles margin is highlighted. It may be significant that the Eastern Somali Basin/Arabian Sea opened more than three times faster than the North Atlantic and twice as fast as the South Atlantic. Current pure passive melting models do not predict any change in oceanic crustal thickness with spreading rate, except at ultra slow seafloor-spreading rates [*Bown and White*, 1994]. Rather, as the spreading rate increases the flux of mantle across the solidus increases and a constant thickness oceanic crust results [*Niu and Hekinian*, 1997]. However, such models assume 100% melt extraction, and perhaps as the width of the melting region increases this is not achieved in reality. In support of this idea we note that the current catalog of steady state "normal" oceanic thickness (those measured away from continental margins and marked with inverted triangles in Figure 11d) trend toward <6 km crustal thickness for spreading rates above 55 mm/a. It is possible that even if there was a modest thermal anomaly at the Seychelles margin at the time of rifting, because of the rapid plate divergence all the melt generated from the wide melting zone could not be extracted and thickened oceanic crust and other features associated with excess magmatism such as extensive SDRs were not produced.

8. Conclusions

[36] The crustal structure determined at the north Seychelles margin (and its conjugate) is characterized by thin oceanic crust, weak expression of seaward-dipping reflectors, and an earlier, prerift underplate of uncertain age. The plateau itself is underlain by 32 km thick continental crust, without any seismic evidence for a thick layer of extruded basalt on its surface. A significant inference from our work is therefore that the two most commonly cited estimates of the spatial extent of the Deccan onshore-offshore province, those of *White and McKenzie* [1989] and *Coffin and Eldholm* [1994], are too large. The Deccan mantle source cannot have had the ~2500 km diameter, axisymmetric shape commonly depicted in the literature.

[37] The pattern of magmatism observed at the north Seychelles continental margin is very different to that observed at previously studied margins that rifted shortly after the eruption of a near-by onshore flood basalt province. In particular the oceanic crust north of the Seychelles is just 5.2 ± 0.1 km thick, and this remained more or less constant for the first 3 Ma of seafloor spreading. In contrast equivalent margins in the North and South Atlantic have initial oceanic crust that is two and one and a half times thicker, respectively, with normal thickness oceanic crust not being produced until 5–10 Ma after rifting. We conclude that our current understanding of the factors influencing the degree of magmatism during continental breakup is incomplete. We speculate that either the lateral flow of hot material beneath the region was hampered in the Seychelles case, perhaps as the rifted margins did not intersect the center of the Deccan mantle source, or there was incomplete melt extraction from the wide melting region that formed between the rapidly diverging plates. If the latter is correct then the rate of plate separation, as indicated by the initial seafloor-spreading rate, is more important in controlling the volume of magmatism gener-

Figure 11. (a) Relationship between thickness of the earliest formed oceanic crust with plume distance for the selected volcanic margins of the North (closed circles) and South (open circles) Atlantic. The margin reference numbers refer to those given in Table 2. Best-fitting straight lines for the two regions are shown together with their R^2 correlation coefficients. Note how the oceanic crustal thickness formed at the north Seychelles margin is significantly thinner than all other volcanic margins formed at similar distances to the Iceland and Tristan da Cunha plumes. (b) Relationship between thickness of the earliest formed oceanic crust and margin width. Again, the margin reference numbers refer to those given in Table 2. North Atlantic margins are shown with closed circles, South Atlantic margins are shown with open circles, and all other margins are shown with diamonds. Only profiles for which full continental crust thickness was achieved on the profile are plotted. The best-fitting straight line is shown, but note the low R^2 correlation coefficient. (c) Predicted average oceanic crustal velocity versus thickness according to the model of *Holbrook et al.* [2001]. Two scenarios are shown: passive upwelling alone ($\chi = 1$, parameterized according to the melting models of *McKenzie and Bickle* [1988] and *Langmuir et al.* [1992]) and active upwelling (with active to passive upwelling ratios χ of 2 and 4). Dashed lines are mantle potential temperature for the *McKenzie and Bickle* [1988] melting model. According to this model, the Seychelles oceanic crust was formed by passive upwelling only of a nonhot mantle. Results for the distal SE Greenland margins (numbered as per Table 2) and East Pacific Rise at 17°S from *Holbrook et al.* [2001] are shown for comparison. (d) Relationship between initial oceanic crustal thickness and seafloor-spreading rate. Margin symbols as in Figure 11b. For clarity only the non-Atlantic margins are numbered according to the listing in Table 2. The inverted triangles mark a global compilation of the thickness of "normal" oceanic crust (i.e., measured away from the immediate passive margin zone, plume traces, and fracture zones) by *Bown and White* [1994] as updated by *White et al.* [2001] and *Minshull et al.* [2001]. The dashed lines show the predicted steady state oceanic crustal thickness according to the passive melting model of *Bown and White* [1994].

ated during continental rifting than has been previously recognized.

[38] **Acknowledgments.** We thank everyone who sailed on *RRS* Charles Darwin cruises CD134b and CD144 and the many people who helped with the installation and running of the land stations. Patrick Joseph of the Seychelles National Oil Company provided access to commercial seismic and magnetic data from the plateau; Bob Fisher of Scripps Institution of Oceanography provided an unpublished, hand-contoured bathymetric chart of the Seychelles region; Ed Stephens of St. Andrews University provided magnetic measurements for a variety of Seychelles rock samples; and Bob White of Cambridge University provided access to the passive melting code. Fiona Hall, Mark Vardy, and Mikhail Evain helped with the data analysis. The seismic data were processed using ProMax software available via a software grant to Imperial College London from Landmark Graphics. This work was funded by the UK Natural Environment Research Council grants NER/A/S/2000/01332, NER/A/S/2000/01390 and NER/A/S/2000/01391, and access to the OBS was via European Union Human Capacity grant HPRI-CT-1999-00037. We thank Douglas Toomey, Keith Louden, and Daniel Lizarralde for their constructive reviews.

References

Anderson, D. L. (1994), The sublithospheric mantle as the source of continental flood basalts: The case against the Continental lithosphere and plume head reservoirs, *Earth Planet. Sci. Lett.*, *123*(1–3), 269–280, doi:10.1016/0012-821X(94)90273-9.

Armitage, J. J., T. J. Henstock, T. A. Minshull, and J. R. Hopper (2008), Modelling the composition of melts formed during continental breakup of the Southeast Greenland margin, *Earth Planet. Sci. Lett.*, *269*(1–2), 248–258, doi:10.1016/j.epsl.2008.02.024.

Barton, A. J., and R. S. White (1997), Crustal structure of Edoras Bank continental margin and mantle thermal anomalies beneath the North Atlantic, *J. Geophys. Res.*, *102*(B2), 3109–3129, doi:10.1029/96JB03387.

Bauer, K., S. Neben, B. Schreckenberger, R. Emmermann, K. Hinz, N. Fechner, K. Gohl, A. Schulze, R. B. Trumbull, and K. Weber (2000), Deep structure of the Namibia continental margin as derived from integrated geophysical studies, *J. Geophys. Res.*, *105*(B11), 25,829–25,853, doi:10.1029/2000JB900227.

Bown, J. W., and R. S. White (1994), Variation with spreading rate of oceanic crustal thickness and geochemistry, *Earth Planet. Sci. Lett.*, *121*(3–4), 435–449, doi:10.1016/0012-821X(94)90082-5.

Bullock, A. D., and T. A. Minshull (2005), From continental extension to seafloor spreading: Crustal structure of the Goban Spur rifted margin, southwest of the UK, *Geophys. J. Int.*, *163*(2), 527–546, doi:10.1111/j.1365-246X.2005.02726.x.

Campbell, I. H. (2007), Testing the plume theory, *Chem. Geol.*, *241*(3–4), 153–176, doi:10.1016/j.chemgeo.2007.01.024.

Chang, H. K., R. O. Kowsmann, A. M. F. Figueiredo, and A. A. Bender (1992), Tectonics and stratigraphy of the East Brazil rift system: An overview, *Tectonophysics*, *213*(1–2), 97–138, doi:10.1016/0040-1951(92)90253-3.

Chian, D. P., and K. E. Louden (1994), The continent-ocean crustal transition across the southwest Greenland margin, *J. Geophys. Res.*, *99*(B5), 9117–9135, doi:10.1029/93JB03404.

Chian, D. P., K. E. Louden, and I. Reid (1995), Crustal structure of the Labrador Sea conjugate margin and implications for the formation of nonvolcanic continental margins, *J. Geophys. Res.*, *100*(B12), 24,239–24,253, doi:10.1029/95JB02162.

Chian, D., I. D. Reid, and H. R. Jackson (2001), Crustal structure beneath Orphan Basin and implications for nonvolcanic continental rifting, *J. Geophys. Res.*, *106*(B6), 10,923–10,940, doi:10.1029/2000JB900422.

Christensen, N. I., and W. D. Mooney (1995), Seismic velocity structure and composition of the continental crust: A global review, *J. Geophys. Res.*, *100*(B6), 9761–9788, doi:10.1029/95JB00259.

Coffin, M. F., and O. Eldholm (1994), Large igneous provinces: Crustal structure, dimensions, and external consequences, *Rev. Geophys.*, *32*(1), 1–36, doi:10.1029/93RG02508.

Collier, J. S., V. Sansom, O. Ishizuka, R. N. Taylor, T. A. Minshull, and R. B. Whitmarsh (2008), Age of Seychelles-India breakup, *Earth Planet. Sci. Lett.*, *272*, 264–277, doi:10.1016/j.epsl.2008.04.045.

Contrucci, I., F. Klingelhofer, J. Perrot, R. Bartolome, M. A. Gutscher, M. Sahabi, J. Malod, and J. P. Rehault (2004a), The crustal structure of the NW Moroccan continental margin from wide-angle and reflection seismic data, *Geophys. J. Int.*, *159*(1), 117–128, doi:10.1111/j.1365-246X.2004.02391.x.

Contrucci, I., L. Matias, M. Moulin, L. Geli, F. Klingelhofer, H. Nouze, D. Aslanian, J. L. Olivet, J. P. Rehault, and J. C. Sibuet (2004b), Deep structure of the west African continental margin (Congo, Zaire, Angola), between 5°S and 8°S, from reflection/refraction seismics and gravity data, *Geophys. J. Int.*, *158*(2), 529–553, doi:10.1111/j.1365-246X.2004.02303.x.

Courtillot, V. E., and P. R. Renne (2003), On the ages of flood basalt events, *C. R. Geosci.*, *335*(1), 113–140, doi:10.1016/S1631-0713(03)00006-3.

Davies, D., and T. J. G. Francis (1964), The crustal structure of the Seychelles Bank, *Deep Sea Res.*, *11*, 921–927.

Dean, S. M., T. A. Minshull, R. B. Whitmarsh, and K. E. Louden (2000), Deep structure of the ocean-continent transition in the southern Iberia Abyssal Plain from seismic refraction profiles: The IAM-9 transect at 40°20′N, *J. Geophys. Res.*, *105*(B3), 5859–5885, doi:10.1029/1999JB900301.

Duncan, R. A., and R. B. Hargraves (1990), $^{40}Ar/^{39}Ar$ geochronology of basement rocks from the Mascarene Plateau, the Chagos Bank and the Maldives Ridge, in *Proceedings of the Ocean Drilling Program: Scientific Results*, vol. 115, edited by R. A. Duncan, J. Backman, and L. C. Peterson, pp. 43–51, Ocean Drill. Program, College Station, Tex.

Duncan, R. A., J. Backman, and L. C. Peterson (Eds.) (1990), *Proceedings of the Ocean Drilling Program: Scientific Results*, vol. 115, Ocean Drill. Program, College Station, Tex.

Eldholm, O., et al. (1986), Dipping reflectors in the Norwegian Sea: ODP Leg 104 drilling results, *J. Geol. Soc.*, *143*(6), 911–912, doi:10.1144/gsjgs.143.6.0911.

Ferněndez-Viejo, G., J. Gallart, J. A. Pulgar, J. Gallastegui, J. J. Dãnobeitia, and D. Córdoba (1998), Crustal transition between continental and oceanic domains along the North Iberian margin from wide angle seismic and gravity data, *Geophys. Res. Lett.*, *25*(23), 4249–4252, doi:10.1029/1998GL900149.

Flueh, E. R., and J. Bialas (1996), A digital, high data capacity ocean bottom recorder for seismic investigations, *Int. Underwater Syst. Design*, *18*(3), 18–20.

Fowler, S. R., R. S. White, G. D. Spence, and G. K. Westbrook (1989), The Hatton Bank continental-margin. Part 2. Deep-structure from 2-ship expanding spread seismic profiles, *Geophys. J.*, *96*(2), 295–309.

Francis, T. J. G., and G. G. Shor (1966), Seismic refraction measurements in the northwest Indian Ocean, *J. Geophys. Res.*, *71*(2), 427–449.

Francis, T. J. G., D. Davies, and M. N. Hill (1966), Crustal structure between Kenya and the Seychelles, *Philos. Trans. R. Soc. London Ser. A*, *259*, 240–261.

Franke, D., S. Neben, B. Schreckenberger, A. Schulze, M. Stiller, and C. M. Krawczyk (2006), Crustal structure across the Colorado Basin, offshore Argentina, *Geophys. J. Int.*, *165*(3), 850–864, doi:10.1111/j.1365-246X.2006.02907.x.

Funck, T., J. R. Hopper, H. C. Larsen, K. E. Louden, B. E. Tucholke, and W. S. Holbrook (2003), Crustal structure of the ocean-continent transition at Flemish Cap: Seismic refraction results, *J. Geophys. Res.*, *108*(B11), 2531, doi:10.1029/2003JB002434.

Funck, T., H. R. Jackson, K. E. Louden, S. A. Dehler, and Y. Wu (2004), Crustal structure of the northern Nova Scotia rifted continental margin (eastern Canada), *J. Geophys. Res.*, *109*, B09102, doi:10.1029/2004JB003008.

Gaedicke, C., H. U. Schluter, H. A. Roeser, A. Prexl, B. Schreckenberger, H. Meyer, C. Reichert, P. Clift, and S. Amjad (2002), Origin of the northern Indus Fan and Murray Ridge, northern Arabian Sea: Interpretation from seismic and magnetic imaging, *Tectonophysics*, *355*(1–4), 127–143, doi:10.1016/S0040-1951(02)00137-3.

Gaskell, T. F., M. N. Hill, and J. C. Swallow (1958), Seismic measurements made by H.M.S. Challenger in the Atlantic, Pacific and Indian Oceans and in the Mediterranean Sea, 1950–53, *Philos. Trans. R. Soc. London Ser. A*, *251*, 23–83, doi:10.1098/rsta.1958.0008.

Goldschmidt-Rokita, A., K. J. F. Hansch, H. B. Hirschleber, T. Iwasaki, T. Kanazawa, H. Shimamura, and M. A. Sellevoll (1994), The ocean continent transition along a profile through the Lofoten Basin, northern Norway, *Mar. Geophys. Res.*, *16*(3), 201–224, doi:10.1007/BF01237514.

Gradstein, F. M., J. G. Ogg, and A. G. Smith (2005), *A Geologic Time Scale 2004*, 610 pp., Cambridge Univ. Press, Cambridge, U. K.

Greenroyd, C. J., C. Peirce, M. Rodger, A. B. Watts, and R. W. Hobbs (2007), Crustal structure of the French Guiana margin, west equatorial Atlantic, *Geophys. J. Int.*, *169*(3), 964–987, doi:10.1111/j.1365-246X.2007.03372.x.

Hammond, J. O. S., J.-M. Kendall, G. Rumpker, J. Wookey, N. Teanby, P. R. Joseph, T. M. Ryberg, and G. Stuart (2005), Upper-mantle anisotropy beneath the Seychelles microcontinent, *J. Geophys. Res.*, *110*, B11401, doi:10.1029/2005JB003757.

Harry, D. L., and D. S. Sawyer (1992), Basaltic volcanism, mantle plumes, and the mechanics of rifting: The Paraná flood-basalt province of South

America, *Geology*, *20*(3), 207–210, doi:10.1130/0091-7613(1992)020<0207:BVMPAT>2.3.CO;2.

Helffrich, G. (2006), Extended-time multi-taper frequency domain cross-correlation receiver function estimation, *Bull. Seismol. Soc. Am.*, *96*, 344–347, doi:10.1785/0120050098.

Hinz, K. (1981), A hypothesis on terrestrial catastrophes: Wedges of very thick oceanward dipping layers beneath passive continental margins - their origin and paleoenvironmental significance, *Geol. Jahrb.*, *E22*, 3–28.

Holbrook, W. S., G. M. Purdy, R. E. Sheridan, L. Glover, M. Talwani, J. Ewing, and D. Hutchinson (1994a), Seismic structure of the US mid-Atlantic continental-margin, *J. Geophys. Res.*, *99*(B9), 17,871–17,891, doi:10.1029/94JB00729.

Holbrook, W. S., E. C. Reiter, G. M. Purdy, D. Sawyer, P. L. Stoffa, J. A. Austin, J. Oh, and J. Makris (1994b), Deep structure of the U.S. Atlantic continental margin, offshore South Carolina, from coincident ocean bottom and multichannel seismic data, *J. Geophys. Res.*, *99*(B5), 9155–9178, doi:10.1029/93JB01821.

Holbrook, W. S., et al. (2001), Mantle thermal structure and active upwelling during continental breakup in the North Atlantic, *Earth Planet. Sci. Lett.*, *190*(3–4), 251–262, doi:10.1016/S0012-821X(01)00392-2.

Hooper, P. R. (1990), The timing of crustal extension and the eruption of continental flood basalts, *Nature*, *345*(6272), 246–249, doi:10.1038/345246a0.

Hopper, J. R., et al. (1992), Magmatism and rift margin evolution: Evidence from northwest Australia, *Geology*, *20*(9), 853, doi:10.1130/0091-7613(1992)020<0853:MARMEE>2.3.CO;2.

Houseman, G. A. (1990), The thermal structure of mantle plumes: Axisymmetric or triple-junction, *Geophys. J. Int.*, *102*(1), 15–24, doi:10.1111/j.1365-246X.1990.tb00527.x.

Keen, C. E., and R. R. Boutilier (2000), Interaction of rifting and hot horizontal plume sheets at volcanic margins, *J. Geophys. Res.*, *105*(B6), 13,375–13,387, doi:10.1029/2000JB900027.

Kelemen, P. B., and W. S. Holbrook (1995), Origin of thick, high-velocity igneous crust along the U.S. East Coast Margin, *J. Geophys. Res.*, *100*(B6), 10,077–10,094, doi:10.1029/95JB00924.

Krishna, K. S., D. G. Rao, and D. Sar (2006), Nature of the crust in the Laxmi Basin (14°–20°N), western continental margin of India, *Tectonics*, *25*, TC1006, doi:10.1029/2004TC001747.

Lane, C. I. (2006), Rifted margin formation in the northwest Indian Ocean: The extensional and magmatic history of the Laxmi Ridge continental margin, Ph.D. thesis, Univ. of Southampton, Southampton, U. K.

Langmuir, C. H., E. M. Klein, and T. Plank (1992), Petrological systematics of mid-ocean ridge basalts: Constraints on melt generation beneath ocean ridges, in *Mantle Flow and Melt Generation at Mid-Ocean Ridges*, *Geophys. Monogr. Ser.*, vol. 71, edited by J. P. Morgan, D. K. Blackman, and J. M. Sinton, pp. 183–280, AGU, Washington, D. C.

Langston, C. A. (1979), Structure under Mount Rainier, Washington, inferred from teleseismic body waves, *J. Geophys. Res.*, *84*, 4749–4762, doi:10.1029/JB084iB09p04749.

Lau, K. W. H., K. E. Louden, T. Funck, B. E. Tucholke, W. S. Holbrook, J. R. Hopper, and H. C. Larsen (2006), Crustal structure across the Grand Banks-Newfoundland Basin continental margin: Part I. Results from a seismic refraction profile, *Geophys. J. Int.*, *167*(1), 127–156, doi:10.1111/j.1365-246X.2006.02988.x.

Lizarralde, D., et al. (2007), Variation in styles of rifting in the Gulf of California, *Nature*, *448*(7152), 466–469, doi:10.1038/nature06035.

Ludwig, W. J., J. E. Nafe, and C. L. Drake (1970), Seismic refraction, in *The Sea: New Concepts of Seafloor Evolution*, vol. 4, edited by A. E. Maxwell, pp. 53–84, Wiley, New York.

Malod, J. A., L. Droz, B. M. Kemal, and P. Patriat (1997), Early spreading and continental to oceanic basement transition beneath the Indus deep-sea fan: Northeastern Arabian Sea, *Mar. Geol.*, *141*(1–4), 221–235, doi:10.1016/S0025-3227(97)00074-1.

McKenzie, D. P., and M. Bickle (1988), The volume and composition of melt generated by extension of the lithosphere, *J. Petrol.*, *29*, 625–679.

Miles, P. R., and W. R. Roest (1993), Earliest seafloor spreading magnetic anomalies in the north Arabian Sea and the ocean-continent transition, *Geophys. J. Int.*, *115*, 1025–1031, doi:10.1111/j.1365-246X.1993.tb01507.x.

Minshull, T. A., S. M. Dean, R. S. White, and R. B. Whitmarsh (2001), Anomalous melt production after continental breakup in the southern Iberia Abyssal Plain, in *Non-Volcanic Rifting of Continental Margins: A Comparison of Evidence from Land and Sea*, edited by R. C. L. Wilson, R. B. Whitmarsh, B. Taylor, and N. Froitzheim, pp. 537–550, Geol. Soc. of London, London.

Minshull, T. A., C. I. Lane, J. S. Collier, and R. B. Whitmarsh (2008), Rifting and magmatism in the northeastern Arabian Sea, *Nat. Geosci.*, *1*(7), 463–467, doi:10.1038/ngeo228.

Mjelde, R., M. A. Sellevoll, H. Shimamura, T. Iwasaki, and T. Kanazawa (1992), A crustal study off Lofoten, N. Norway, by use of 3-component ocean bottom seismographs, *Tectonophysics*, *212*(3–4), 269–288, doi:10.1016/0040-1951(92)90295-H.

Mjelde, R., T. Raum, B. Myhren, H. Shimamura, Y. Murai, T. Takanami, R. Karpuz, and U. Naess (2005), Continent-ocean transition on the Voring Plateau, NE Atlantic, derived from densely sampled ocean bottom seismometer data, *J. Geophys. Res.*, *110*, B05101, doi:10.1029/2004JB003026.

Mohriak, W. U., M. Bassetto, and I. S. Vieira (1998), Crustal architecture and tectonic evolution of the Sergipe-Alagoas and Jacuipe basins, offshore northeastern Brazil, *Tectonophysics*, *288*(1–4), 199–220, doi:10.1016/S0040-1951(97)00294-1.

Muller, R. D., M. Sdrolias, C. Gaina, and W. R. Roest (2008), Age, spreading rates, and spreading asymmetry of the world's ocean crust, *Geochem. Geophys. Geosyst.*, *9*, Q04006, doi:10.1029/2007GC001743.

Mutter, J. C., and R. L. Larson (1989), Extension of the Exmouth Plateau, offshore northwestern Australia: Deep seismic reflection/refraction evidence for simple and pure shear mechanisms, *Geology*, *17*(1), 15–18, doi:10.1130/0091-7613(1989)017<0015:EOTEPO>2.3.CO;2.

Mutter, J. C., and C. M. Zehnder (1988), Deep crustal structure and magmatic processes: The inception of seafloor spreading in the Norwegian-Greenland Sea, in *Early Tertiary Volcanism and the Opening of the NE Atlantic*, edited by A. C. Morton and L. M. Parson, pp. 35–48, Geol. Soc. of London, London.

Mutter, J. C., W. R. Buck, and C. M. Zehnder (1988), Convective partial melting: 1. A model for the formation of thick basaltic sequences during the initiation of spreading, *J. Geophys. Res.*, *93*(B2), 1031–1048, doi:10.1029/JB093iB02p01031.

Naini, B. R., and M. Talwani (1982), Structural framework and the evolutionary history of the continental margin of western India, in *Studies in Continental Margin Geology*, edited by J. S. Watkins and C. L. Drake, pp. 167–191, Am. Assoc. of Pet. Geol., Tulsa, Okla.

Nielsen, T. K., and J. R. Hopper (2004), From rift to drift: Mantle melting during continental breakup, *Geochem. Geophys. Geosyst.*, *5*, Q07003, doi:10.1029/2003GC000662.

Nielsen, T. K., H. C. Larsen, and J. R. Hopper (2002), Contrasting rifted margin styles south of Greenland: Implications for mantle plume dynamics, *Earth Planet. Sci. Lett.*, *200*(3–4), 271–286, doi:10.1016/S0012-821X(02)00616-7.

Nissen, S. S., D. E. Hayes, P. Buhl, J. Diebold, B. C. Yao, W. J. Zeng, and Y. Q. Chen (1995), Deep penetration seismic-soundings across the northern margin of the South China Sea, *J. Geophys. Res.*, *100*(B11), 22,407–22,433, doi:10.1029/95JB01866.

Niu, Y. L., and R. Hekinian (1997), Spreading-rate dependence of the extent of mantle melting beneath ocean ridges, *Nature*, *385*(6614), 326–329, doi:10.1038/385326a0.

Norton, I. O., and J. G. Sclater (1979), A model for the evolution of the Indian Ocean and the breakup of Gondwanaland, *J. Geophys. Res.*, *84*(B12), 6803–6830, doi:10.1029/JB084iB12p06803.

Olafsson, I., E. Sundvor, O. Eldholm, and K. Grue (1992), Møre margin: Crustal structure from analysis of expanded spread profiles, *Mar. Geophys. Res.*, *14*(2), 137–162, doi:10.1007/BF01204284.

Peate, D. W., C. J. Hawkesworth, M. S. M. Mantovani, and W. Shukowsky (1990), Mantle plumes and flood-basalt stratigraphy in the Paraná, South America, *Geology*, *18*(12), 1223–1226, doi:10.1130/0091-7613(1990)018<1223:MPAFBS>2.3.CO;2.

Planke, S., and O. Eldholm (1994), Seismic response and construction of seaward dipping wedges of flood basalts: Voring volcanic margin, *J. Geophys. Res.*, *99*(B5), 9263–9278, doi:10.1029/94JB00468.

Planke, S., P. A. Symonds, E. Alvestad, and J. Skogseid (2000), Seismic volcanostratigraphy of large-volume basaltic extrusive complexes on rifted margins, *J. Geophys. Res.*, *105*(B8), 19,335–19,351, doi:10.1029/1999JB900005.

Plummer, P. S. (1994), Mesozoic source rocks and hydrocarbon potential of the Seychelles offshore, *J. Pet. Geol.*, *17*(2), 157–176, doi:10.1111/j.1747-5457.1994.tb00124.x.

Plummer, P. S. (1996), The Amirante ridge/trough complex: Response to rotational transform rift drift between Seychelles and Madagascar, *Terra Nova*, *8*(1), 34–47, doi:10.1111/j.1365-3121.1996.tb00723.x.

Randall, G. E. (1989), Efficient calculation of differential seismograms for lithospheric receiver functions, *Geophys. J. Int.*, *99*, 469–481, doi:10.1111/j.1365-246X.1989.tb02033.x.

Reddy, P. R. (2005), Crustal velocity structure of western India and its use in understanding intraplate seismicity, *Curr. Sci.*, *88*(10), 1652–1657.

Richards, M. A., R. A. Duncan, and V. E. Courtillot (1989), Flood basalts and hot-spot tracks: Plume heads and tails, *Science*, *246*(4926), 103–107, doi:10.1126/science.246.4926.103.

Royer, J. Y., A. K. Chaubey, J. Dyment, G. C. Bhattacharya, K. Shrinivas, V. Yatheesh, and T. Ramprasad (2002), Paleogene plate tectonic evolu-

tion of the Arabian Sea and eastern Somali Basin, *Geol. Soc. Spec. Publ.*, *195*, 7–23.

Sandwell, D. T., and W. H. F. Smith (1997), Marine gravity anomaly from Geosat and ERS-1 satellite altimetry, *J. Geophys. Res.*, *102*, 10,039–10,054, doi:10.1029/96JB03223.

Sansom, V. (2006), Crustal structure of the NE Seychelles rifted continental margin from geophysical observations, Ph.D. thesis, Imperial College, London.

Shor, G. G., and D. D. Pollard (1963), Seismic investigations of Seychelles and Saya de Malha Banks, northwest Indian Ocean, *Science*, *142*, 48–49, doi:10.1126/science.142.3588.48.

Sleep, N. H. (1997), Lateral flow and ponding of starting plume material, *J. Geophys. Res.*, *102*(B5), 10,001–10,012, doi:10.1029/97JB00551.

Sleep, N. H. (2007), Edge-modulated stagnant-lid convection and volcanic passive margins, *Geochem. Geophys. Geosyst.*, *8*, Q12004, doi:10.1029/2007GC001672.

Talwani, M., J. L. Worzel, and M. Landisman (1959), Rapid gravity computations for two-dimensional bodies with application to the Medocino submarine fracture zone, *J. Geophys. Res.*, *64*, 49–59, doi:10.1029/JZ064i001p00049.

Todal, A., and O. Edholm (1998), Continental margin off western India and Deccan large igneous province, *Mar. Geophys. Res.*, *20*(4), 273–291, doi:10.1023/A:1004640508371.

van Wijk, J. W., R. S. Huismans, M. ter Voorde, and S. Cloetingh (2001), Melt generation at volcanic continental margins: No need for a mantle plume?, *Geophys. Res. Lett.*, *28*(20), 3995–3998, doi:10.1029/2000GL012848.

Vogt, U., J. Makris, B. M. O'Reilly, F. Hauser, P. W. Readman, A. W. B. Jacob, and P. M. Shannon (1998), The Hatton basin and continental margin: Crustal structure from wide-angle seismic and gravity data, *J. Geophys. Res.*, *103*(B6), 12,545–12,566, doi:10.1029/98JB00604.

Voss, M., and W. Jokat (2007), Continent-ocean transition and voluminous magmatic underplating derived from P wave velocity modelling of the east Greenland continental margin, *Geophys. J. Int.*, *170*(2), 580–604, doi:10.1111/j.1365-246X.2007.03438.x.

Wegener, A. (1924), *The Origins of Continents and Oceans*, 212 pp., Methuen, London.

White, R. S. (1992a), Crustal structure and magmatism of North Atlantic continental margins, *J. Geol. Soc.*, *149*, 841–854, doi:10.1144/gsjgs.149.5.0841.

White, R. S. (1992b), Magmatism and the causes of continental breakup, *Geol. Soc. Spec. Publ.*, *68*, 1–16.

White, R. S., and D. McKenzie (1989), Magmatism at rift zones: The generation of volcanic continental margins and flood basalts, *J. Geophys. Res.*, *94*(B6), 7685–7729, doi:10.1029/JB094iB06p07685.

White, R. S., and D. McKenzie (1995), Mantle plumes and flood basalts, *J. Geophys. Res.*, *100*(B9), 17,543–17,585, doi:10.1029/95JB01585.

White, R. S., D. McKenzie, and R. K. O'Nions (1992), Oceanic crustal thickness from seismic measurements and rare-earth element inversions, *J. Geophys. Res.*, *97*(B13), 19,683–19,715, doi:10.1029/92JB01749.

White, R. S., T. A. Minshull, M. J. Bickle, and C. J. Robinson (2001), Melt generation at very slow-spreading oceanic ridges: Constraints from geochemical and geophysical data, *J. Petrol.*, *42*(6), 1171–1196, doi:10.1093/petrology/42.6.1171.

Whitmarsh, R. B., R. S. White, S. J. Horsefield, J. C. Sibuet, M. Recq, and V. Louvel (1996), The ocean-continent boundary off the western continental margin of Iberia: Crustal structure west of Galicia Bank, *J. Geophys. Res.*, *101*(B12), 28,291–28,314, doi:10.1029/96JB02579.

Whitmarsh, R. B., T. A. Minshull, S. M. Russell, S. M. Dean, K. E. Louden, and D. P. Chian (2001), The role of syn-rift magmatism in the rift-to-drift evolution of the west Iberia continental margin: Geophysical observations, in *Non-Volcanic Rifting of Continental Margins: A Comparison of Evidence From Land and Sea*, edited by R. C. L. Wilson et al., pp. 107–124, Geol. Soc. of London, London.

Zelt, C. A. (1999), Modelling strategies and model assessment for wide-angle seismic traveltime data, *Geophys. J. Int.*, *139*(1), 183–204, doi:10.1046/j.1365-246X.1999.00934.x.

Zelt, C. A., and P. J. Barton (1998), Three-dimensional seismic refraction tomography: A comparison of two methods applied to data from the Faeroe Basin, *J. Geophys. Res.*, *103*(B4), 7187–7210, doi:10.1029/97JB03536.

Zelt, C. A., and D. A. Forsyth (1994), Modeling wide-angle seismic data for crustal structure: Southeastern Grenville Province, *J. Geophys. Res.*, *99*(B6), 11,687–11,704, doi:10.1029/93JB02764.

Zelt, C. A., and R. B. Smith (1992), Seismic traveltime inversion for 2-D crustal velocity structure, *Geophys. J. Int.*, *108*(1), 16–34, doi:10.1111/j.1365-246X.1992.tb00836.x.

Zhu, L., and H. Kanamori (2000), Moho depth variation in southern California from teleseismic receiver functions, *J. Geophys. Res.*, *105*(B2), 2969–2980, doi:10.1029/1999JB900322.

J. S. Collier and V. Sansom, Department of Earth Science and Engineering, Imperial College London, South Kensington Campus, London SW7 2AZ, UK. (jenny.collier@ic.ac.uk)

J. O. S. Hammond and J.-M. Kendall, Department of Earth Sciences, University of Bristol, Wills Memorial Building, Queen's Road, Bristol BS8 1RJ, UK.

C. I. Lane, T. A. Minshull, and R. B. Whitmarsh, National Oceanography Centre, University of Southampton, Waterfront Campus, European Way, Southampton SO14 3ZH, UK.

G. Rumpker, Arbeitsbereich Geophysik, Johann Wolfgang Goethe Universitat, Altenhöferallee 1, D-60438 Frankfurt, Germany.